BEAMLINE AND ACCELERATOR DEVELOPMENT

Report on Beam Line Status

R. Blue, R. Ronningen, E. Kashy

The beam lines for Phase I operation have been assembled up to the isolation valves at the various experimental stations. Two lines have been completed, that for the 60-inch scattering chamber and for the gamma-ray goniometer chamber. Most of the vacuum hardware is aluminum with indium wire seals. Marmon flanges are employed on demountable joints. Vacuum pumping requirements are met by 60 liter/sec. triode ion pumps located at 8-10 foot intervals along the beam lines and by 1000 liter/sec. cryopumps on each of the two magnet chambers.

The beam lines are now maintained under vacuum in the low 10^{-7} Torr range or better. A slight further improvement is expected when the Viton O-rings installed temporarily on several beam box ports are replaced by metal C-seals.

Extensive use has been made of components salvaged from the K-50 cyclorton beam lines including pipe sections, beam boxes, quadrupole magnets, and dipole magnets. Purchased components include the gate valves and the vacuum pumps. The major items which have been fabricated for the new beam lines are the vacuum chambers for the two dipole magnets and beam box modules (slits, stops, and viewers).

A beam collimating slit edge module is shown in Fig. 1. Twelve of these modules have been assembled, wired, and vacuum tested. The wide variation in the range for particles to be accelerated at this facility made the choice of shape for the slit edge difficult. The selected design uses 1100 aluminum with a total thickness of 1.12 inches. The leading and trailing edges are bevelled at 2.5° angle over 0.45 inches leaving a central flat region of 0.22 inches. Each slit edge is remotely adjustable over a one inch range. A closed - circuit water cooling system for slits and stops in presently being tested on one beam box.

Fig. 2 and 3 show a beam stop and a beam viewer, respectively. Work remaining on these modules includes some wiring and the production of a sufficient number of the standard modules that interface these devices, via CAMAC, to the computer control system. Most of the required cabling is in place.

The beam - handling magnetic elements have been installed except near the K-500 exit where studies of the extracted beam will be made before the final beam line is constructed. Operational testing of power supplies and controls has been completed for all magnetic elements up to the switching magnet.

A standard control panel for the operation of beam line vacuum values has been designed

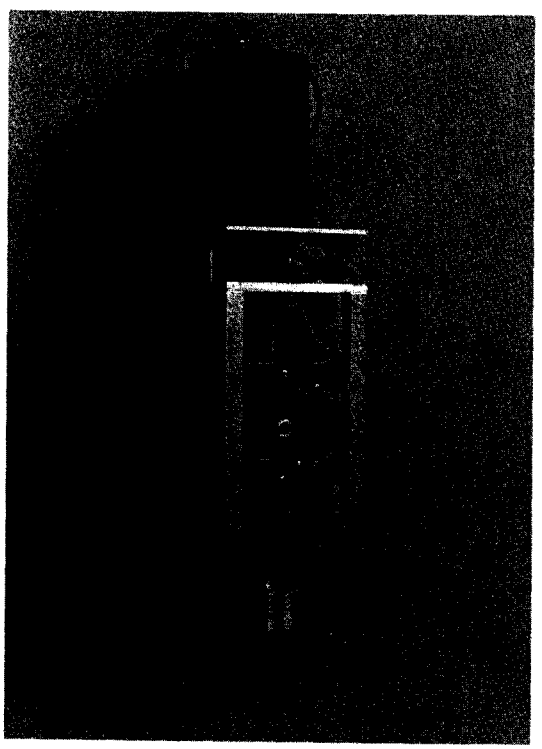

Fig. 1. Slit Edge Module.

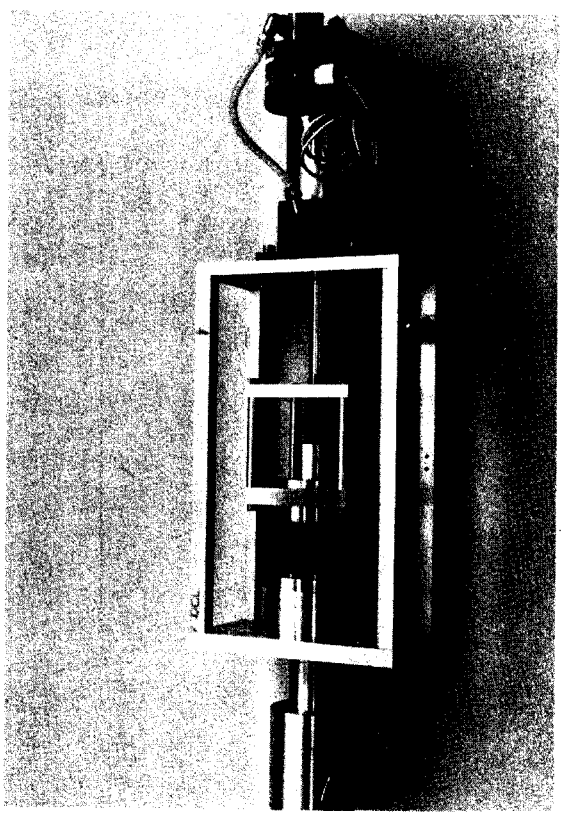

Fig. 2. Beam stop.

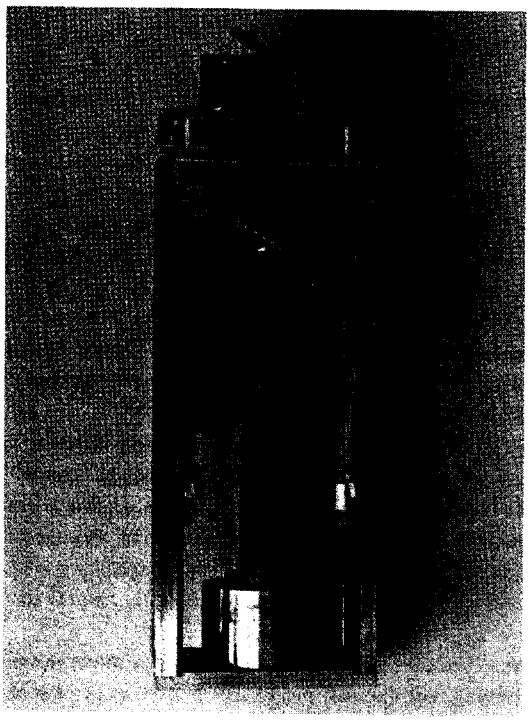

Fig. 3. Beam viewer.

and one unit has been built for testing. The interlock logic designed to protect against vacuum failures will be handled by a Modicon programmable controller. This design approach provides complete flexibility for setting interlock requirements including the conditions under which the interlocks may be by-passed. Remote control of the valves and the sensing of their status can also be provided via the K-500 console control computer.

Most of the devices and interlocks relating to radiation safety have been installed and are operational. These include a system of area radiation monitors, shielding doors, and wall plugs. The area monitor system uses cadmium-wrapped, parafine - moderated BF_3 counters located in each vault and at key locations outside shield walls. In addition two Geiger counter survey meters have been mounted near exits from the shielded area to provide a means for convenient check of induced activity in materials exposed to radiation.

Neutron Shielding Calculations for Phase II Operations

J. Naryanaswamy, J. Duffy, E. Kashy, Z. Koenig, R.M. Ronningen and F. Sottile

The coupled superconducting cyclotrons will provide experimentalists with a wide range of heavy ion beams (from ^{4}He to ^{238}U), energies (up to 200 MeV/A), and intensities (up to 10^{13} particles/sec.). Beams with these characteristics produce copious amounts of penetrating radiation, the most important being neutrons. A broad spectrum of neutron energies results from interactions with the beam-stopping material. A significant fraction of the neutrons have velocity nearly the same as the beam velocity.

We have completed a report which contains calculations of neutron radiation exposure of laboratory personnel (dose rates) for the expected typical operations of the facility. In doing this, an expected operations mode was first defined: available beams, intensities, and facility usage in terms of target areas and tuning areas. Secondly, models of neutron production in heavy ion reactions were investigated and utilized to predict neutron yields. Finally, dose rates were calculated for key areas within the facility, outside the experimental vaults. Radiation external to the facility from "skyshine" was also estimated.

The major focus of this study was to attain low, short-term, dose rates (<2.5 mRem/hr) just outside shielding walls by designing local iron shielding surrounding beam dumps and stops. This local shielding, when combined with the concrete shielding provided in the facility construction will ensure that the integrated exposure of personnel will be well below the 5 Rem/yr (whole body dose) maximum permissible exposure of radiation workers.

The experimental area floor plan is shown in Fig. 1. The radiation shielding will consist of concrete walls and local iron shielding.

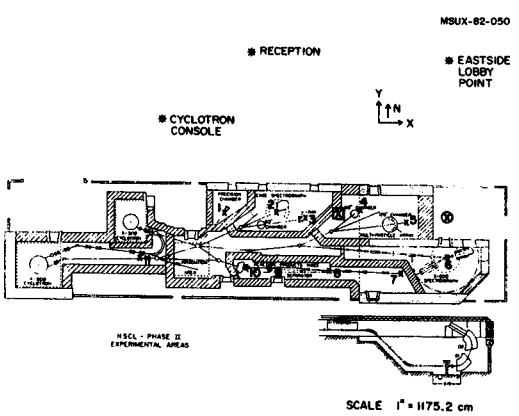

Fig. 1.

Local shielding will be required wherever the beam is stopped, mainly at Faraday cups at the ends of beam lines, and at beam defining slits and stops in the beam transport system. These locations are labeled in the figure and are further specified in Table 1.

TABLE 1. EXPERIMENTAL AREA DESCRIPTION

Experimental Area	Description
1	Precision Chamber
2	Enge Spectrograph
3	Gamma Ray
4	60 In. Chamber
5	120 In. Chamber
6	S-800 Spectrograph
7	RPMS
8	RPMS
9	RPMS
10	RPMS
11	TUNING

A projection of how much time a given beam with a given intensity will be used in each experimental area was then made, and the results are summarized in Table 2. Conservatively, the beam energies and intensities are upper limits. It should be noted that the percent-time/yr adds to 80%; we assume 20% accelerator maintenance time and that the cyclotrons' duty factors are each 100%.

Representative points outside the experimental halls were chosen to study the neutron does rates there. These are the cyclotron console area, the visitor reception area, and an area in the east side lobby. These points are noted in Fig. 1.

We have written a computer code which models the facility operation and calculates in a semi-empirical way the neutron energy spectra at given locations within the laboratory. The code is presently being implemented for interactive usage on the VAX 11/780. For each source (beam stop or dump) the neutron yield is calculated from the production cross section in a "thick target" calculation. This is done for the specific angle to the test point. The concrete thickness of shielding walls is fixed in the input. The yield is further attenuated by the R^{-2} dependence of flux from a point source. This is the well known "Moyer model" for neutron attenuation. The attenuating effect of local shielding is also included. The result is the energy spectrum of neutrons at the test point. The integrated flux and dose rate are than computed.

TABLE 2: PROJECTED BEAM AND EXPERIMENTAL AREA USEAGE IN PHASE II AT NSCL

BEAM	E/A (MeV)	PARTICLE CURRENT	PERCENT TIME/YR.	FRACTIONAL TIME IN EXPERIMENTAL AREAS 1	2	3	4	5	6	7	8	9	10	11
4He	200	1.56×10^{12}	5.0	.0	.0	.0	.40	.00	.40	.00	.00	.0	.0	.20
12C	200	5.20×10^{11}	5.0	.0	.0	.0	.12	.20	.24	.06	.06	.06	.06	.20
16O	200	3.90×10^{11}	10.0	.0	.0	.0	.12	.20	.24	.06	.06	.06	.06	.20
20Ne	200	3.12×10^{11}	15.0	.0	.0	.0	.12	.20	.24	.06	.06	.06	.06	.20
40Ar	200	1.73×10^{11}	15.0	.0	.0	.0	.12	.20	.24	.06	.06	.06	.06	.20
76Ge	125	1.04×10^{11}	7.5	.0	.0	.0	.0	.0	.0	.20	.20	.20	.20	.20
86Kr	105	1.01×10^{11}	7.5	.0	.0	.0	.0	.0	.0	.20	.20	.20	.20	.20
208Pb	20	2.60×10^{10}	7.5	.0	.0	.80	.0	.0	.0	.0	.0	.0	.0	.20
238U	20	2.50×10^{9}	7.5	.0	.0	.80	.0	.0	.0	.0	.0	.0	.0	.20

Our model for energetic neutron production in heavy ion collisions is based on two major mechanisms, namely the "moving thermal source" and projectile fragmentation. For the moving source, one finds, qualitatively, that cross sections for light particle production can be well described in terms of a Maxwellian distribution observed in a rest frame that moves at slightly less than half the beam velocity, once a correction has been made for the Coulomb interaction with the target nucleus. The relativistic expression for the cross section can be written[1]

$$Ed^2\sigma/p^2dpd\Omega = N'_{MS}(E-\beta pcos\theta)\exp[-\gamma(T-\beta pcos\theta)/T_{MS}]. \quad (1)$$

(The variables in Eq. (1) are described below.)

A second mechanism, important for lighter projectiles, and dominant in the forward direction ($\theta \lesssim 40^o$), is projectile fragmentation. Here the source moves in the beam direction with the beam velocity. Combining the two mechanisms, the functional form for the differential cross section obtained is[2]

$$d^2\sigma/d\Omega dE = p\{(Ed^2\sigma/p^2dpd\Omega)_{MS} +$$

$$N'_F\,\gamma'(E-\beta' pcos\theta)\exp[-(p^2(cos^2\theta(\gamma'^2-1)+1)$$

$$+\gamma'^2\beta' E(\beta' E-2pcos\theta))/T_F] .$$

Here, N'_{ms} and N'_F are reaction-dependent quantities that contain target-projectile geometrical factors (given below). The primed quantities are related to the source having the beam velocity. The parameter T_F is 7.5 MeV. It is the effective "temperature" in the fragmentation process, defining the average Fermi energy of a nucleon in nuclear matter; $\beta,\gamma,\beta',\gamma'$ are familiar relativistic kinematical factors, E,p are the energy and momentum of the emitted light particle, θ is the angle of emission, and T_{MS} is the moving source temperature, estimated from existing data.[3] T is kinetic energy.

Data[3-7] for the two processes for beam energies with E/A=20 MeV to 1 GeV were compiled and fitted to determine N'_{MS} and N'_F. Few data exist for the energies that will be available in Phase II, especially for small angles. We fitted existing data for N'_{MS} and N'_F and extrapolated the results to Phase II operations using the semi-empirical geometry and energy dependences of the cross sections.

The model above was developed for light charged particle emission. To use it for neutrons the Coulomb barrier was removed, and the ratio of the number of neutrons to protons in the target was included.

The neutron flux was calculated from the beam stopping in either aluminum (at beam diagnostic points) or in the water Faraday cups. After determining neutron yields at a desired point the dose rates were calculated. Flux density-to-dose-equivalent-rate conversions[8] for neutrons with energies $10\text{-}10^3$ MeV were parameterized by

$$\text{dose rate (mRem/hr)} = \text{flux (n/cm}^2\text{/sec)}/11.615E^{-0.235},$$

where the flux density is taken for neutrons with energy E in MeV. The total dose rate was determined by integrating over the neutron flux energy distribution.

Our model was tested by calculating the neutron energy and angular distribution data[9] for 710 MeV α-particles on water and steel. Calculated and experimental yields for neutrons at 0^o and 45^o were presented in last year's annual report.

To identify beams which produce large numbers of neutrons all beams were studied at a given site (0^o direction for the γ-ray beam line, marked "X" in Fig. 1). The results are given in Table 3. Inspection of this table shows that 150 cm of iron is adequate for ^{12}C beams and those heavier. But, for α particles an additional 50 cm of iron is required, unless the beam intensity is reduced.

In order to obtain a maximum dose rate of 2.5 mRem/hr outside the experimental vaults, shielding local to beam dumps and tuning beam stops is required. The attenuation lengths for neutrons in iron were calculated by using those for concrete and scaling them by the ratio of densities.

Calculations for forward-directed neutrons from 200 MeV/A ^{12}C ions stopping in water show that 150 cm of iron are needed to obtain desired dose-rates. In the transverse directions 75 cm is sufficient. An initial design of the local shield is sketched in Fig. 2. The shielding may be moved from one experimental line to another. Current plans include at least one shield per vault.

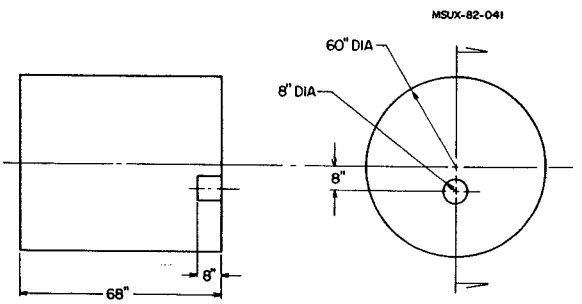

Fig. 2.

Using the information contained in Tables 2 and 3 calculations were done using all beams in all experimental areas, to model the yearly operation. The neutron flux and dose rate were computed for the three test locations. The yearly integrated dose was calculated assuming a 40-hr-week and a 52-week-year. These results are shown in Table 4. It is clear that both the dose rate and yearly integrated dose are well below the maximum permissible values. Certainly one of the first experiments will be to measure neutron flux once the accelerators are operating.

We also estimated the neutron flux at points external and distant (>100 m) from NSCL. This flux is due to direct transmission and atmosphere-scattered neutrons, whose source is taken to be a beam stopping in an iron-shielded water Faraday cup. Neutron flux in the atmospheric medium is known as skyshine.

We considered a severe operating case, viz. the radiation from the 200 MeV/A ^{12}C beam with an intensity of 5.2×10^{11} particles/sec in the 60" scattering chamber area. The shielding against skyshine is from concrete roof beams. We assume that a thickness of 1.37 m will suffice, this being three layers of the standard 18 inch roof beam. A thickness of 75 cm of iron, surrounding the Faraday cup, was assumed even though there can be 150 cm in the very forward direction (based on our study above).

TABLE 3. CALCULATIONS OF DOSE RATES IN FORWARD DIRECTION OUTSIDE OF SHIELD WALL FOR BEAMS STOPPING AT γ-RAY SITE.

Beam	Energy/nucleon (MeV/A)	Particle Current (10^{12}sec^{-1})	Local Shielding Thickness (cm of iron)	Dose-Rate (mRem/hr)
^{4}He	200	1.56	0	1.6×10^{4}
			150	49
			200	0.4
^{12}C	200	0.52	0	5.9×10^{3}
			150	1.8
^{16}O	200	0.39	0	4.0×10^{3}
			150	1.2
^{20}Ne	200	0.31	0	2.9×10^{3}
			150	0.9
^{40}Ar	200	0.17	0	1.4×10^{3}
			150	0.4
^{76}Ge	125	0.10	0	59
			150	1.2×10^{-2}
^{86}Kr	105	0.10	0	18
			150	2.8×10^{-3}
^{208}Pb	20	0.026	0	4.4×10^{-6}
			150	0
^{238}U	20	0.0025	0	4.2×10^{-7}

TABLE 4. YEARLY INTEGRATED DOSE FROM PROJECTED "TYPICAL" FACILITY OPERATIONS.

Area	Neutron Flux (n/cm^2 /sec)	Dose Rate (mRem/hr)	Yearly Integrated Dose (Rem/yr)
Cyclotron Control Console	9.3×10^{-4}	2.5×10^{-4}	5.3×10^{-4}
Reception area	1.6×10^{-1}	9.1×10^{-3}	1.9×10^{-2}
East-side Lobby	1.2×10^{-2}	3.6×10^{-3}	7.5×10^{-3}

An adequate description of the skyshine flux at a point R due to a point source (we used a rectangular, extended source) empirically is given by[8]

$$\chi(R) = (aQ/4\pi R^2)(1-\exp(-R/\mu))\exp(-R/\lambda).$$

Here Q is the source strength (neutrons/sec), and a,μ, and λ are empirically determined constants. This expression is valid for R > 50 m. The behavior at large values of R is dominated by $e^{-R/\lambda}$, so λ is the attenuation length of neutrons in air.

For the case of 200 MeV/A ^{12}C the neutrons have a mean energy (at the upper roof surface) of 150 MeV or so. Thus λ=100 m is appropriate. For 80 MeV and 10 MeV neutrons, μ is 47 and 56 m respectively.[11] So for our purposes we use μ=40 m. The uncertainty in the calculated flux because of uncertainties in μ and λ is estimated to be smaller than 20%. The value of a=2.8 was used.[8]

Some results are shown in Fig. 3. The skyshine flux appears to be very small under the above assumptions.

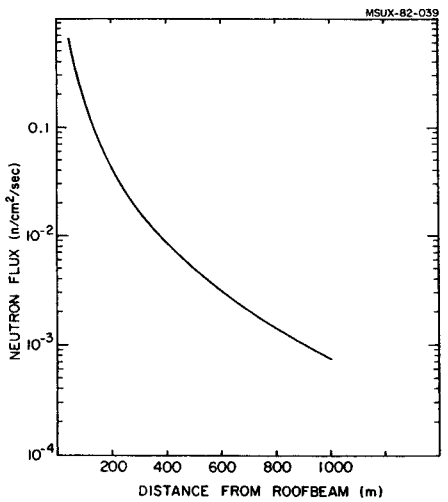

Fig. 3.

1. T.C. Awes, G. Poggi, S. Saini, C.K. Gelbke, R. Legrain, and G.D. Westfall, Phys. Lett. 103B, 417 (1981).
2. G.F. Bertsch and D.K. Scott, private communication.
3. L. Anderson, Ph.D. thesis (unpublished); Lawrence Berkeley Laboratory report LBL-6767 (1977).
4. S. Nagamiya, M.-C. Lemaire, E. Moeller, S. Schnetzer, G. Shapiro, and A. Tanihata, Phys. Rev. C24, 971 (1981).
5. T.C. Awes, S. Saini, G. Poggi, C.K. Gelbke, D. Cha, R. Legrain, and G.D. Westfall, MSUCL-62 (1981).
6. B. Jakobsson, L. Carlen, P. Kristiansson, J. Krumlinde, A. Oskarsson, H.-A. Gustafsson, T. Johansson, H. Ryde, G. Tibell, J.P. Bondorf, G. Fai, A.O.T. Karvinen, O.B. Nielson, M. Buenerd, J. Cole, D. Lebrun, J.M. Loiseaux, P. Martin, R. Ost, P. de Saintignon, C. Guet, E. Monnand, J. Mougey, H. Nifenecker, P. Perrin, J. Pinston, C. Ristori, F. Schussler, Phys. Lett. 102B, 121 (1981).
7. J.R. Wu, C.C. Chang, H.D. Holmgren, and R.W. Koontz, Phys. Rev. C20, 1284 (1979).
8. Accelerator Health Physics, H. Wade Patterson and Ralph H. Thomas (Academic Press, New York) 1973.
9. R.A. Cecil, B.D. Anderson, A.R. Baldwin, R. Madey, A. Galonsky, P. Miller, L. Young, and F.M. Waterman, Phys. Rev. C21, 2471 (1980).

The C-Magnet for the K-500 Cyclotron Exit Port

J. Nolen, M. Distasio, M. Dubois, L.H. Harwood, E. Kashy, and A. Zeller

A small specially shaped magnet is required to steer the various beams extracted from the K-500 cyclotron into the beam transport system. Beam extraction calculations show that although the directions of various beams vary by $\pm 2^{o}$, all beams should pass through a common point 10." outside the cyclotron yoke. A small magnet centered at this location should be adequate to redirect any beam into the first section of the beam transport system. However, it is also essential to locate a beam probe at this same location for external beam diagnostics. As a result of this geometry constraint, a small C-magnet was designed and constructed with the coils wrapped around the yoke to allow unobstructed access to the gap region from one side of the magnet. A photograph of the resulting magnet installed at the cyclotron exit port is shown in Fig. 1. The magnet parameters and the results of field measurements are given in the Table and Fig. 2 and 3.

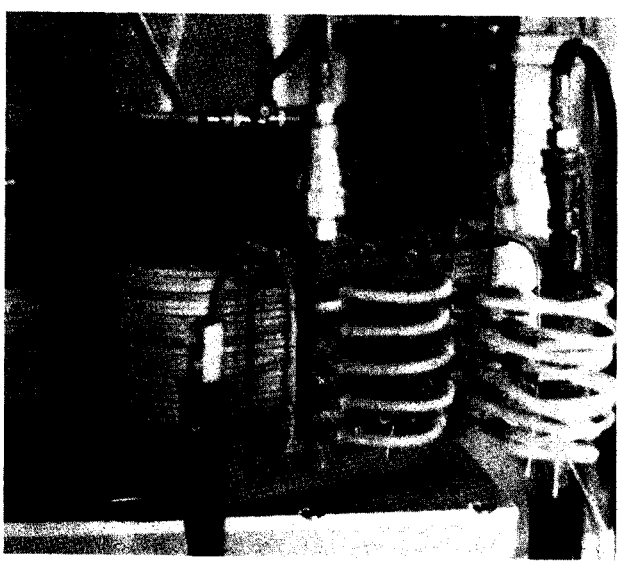

Fig. 1. A photograph of the C-magnet installed at the K-500 cyclotron exit port. The magnet coils are wrapped around the return yoke on the near side of the picture. The rectangular beam tube from the cyclotron is entering the C-magnet on the left side.

MSUX-82-415

a)

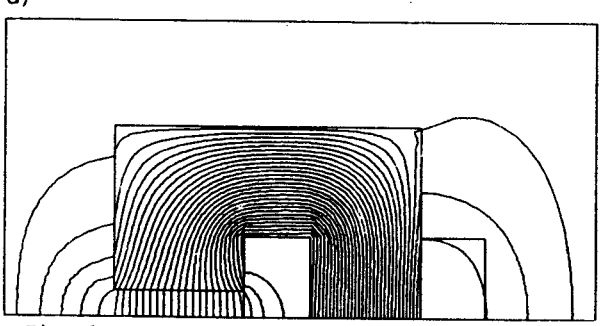

Fig. 2. a) A two dimensional magnetic field map calculated for the C-magnet using the program POISSON.

MSUX-82-414

b)

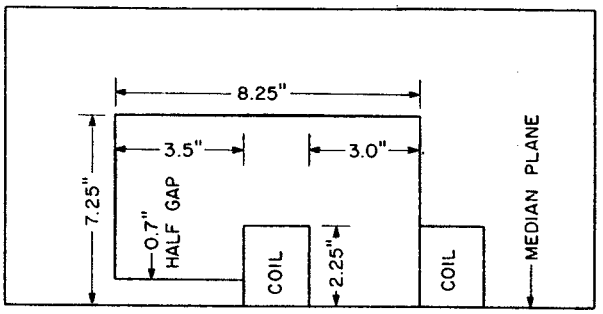

Fig. 2. b) A section showing the dimension of the C-magnet perpendicular to the beam. The magnet is 10.25" along the beam.

Table I: Parameters of the C-Magnet for the k-500 Cyclotron Exit Port.

Magnet gap:	1.4"
Gap width:	3.5"
Pole tip length:	10.25"
Number of turns:	160
Maximum current:	150a
Maximum voltage:	$21.V_{o}$
Maximum field:	5.9 kG
Cooling water:	0.4 gal/min
Conductor size:	3/16" square x 0.090" diameter hole.
Steel:	AISI C1018 Cold finished
Power requirements @ 5.5 kG:	110a @ 15 V
Field flatness:	$\Delta B/B \leq 10^{-3}$ over 1" wide central region

MSUX-82-383

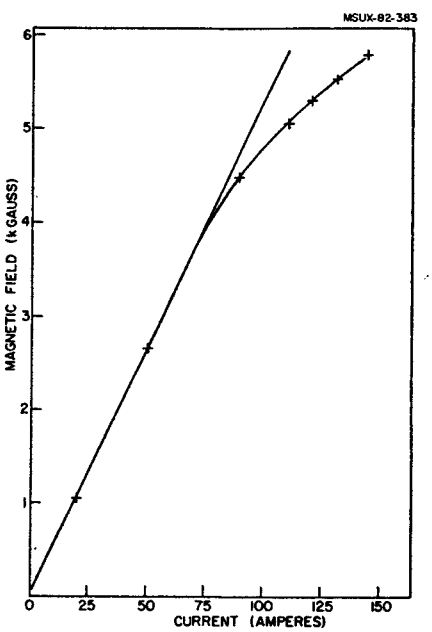

Fig. 3. The measured central field of the C-magnet vs. coil current. The effects of saturation are extensive. At 120 amps the gap limited field is 6.78 kG, the POISSON calculated field (2 dimensional) is 6.2 kG, while the actually measured field is 5.35 kG.

The field measurements on this magnet produced the surprising result that the magnet saturates at a field much lower than calculated with the 2-dimensional code POISSON. It was known that this magnet is less efficient than a standard C-magnet with the coils wrapped around the pole tips, but it was expected that this effect would be largely accounted for by the 2-dimensional calculation. Since we have come to rely on such POISSON calculations in the specifications of so many other magnets, we were disturbed by this discrepancy. Below we consider a simple model for the 3-dimension aspects of the fields to see if they are responsible for the problem.

In Fig. 4 the median planes of this C-magnet and a standard C-magnet are schematically represented. This simple comparison illustrates one important qualitative difference between the two designs. In the standard design, with the coils around the pole tips, the external fields outside the coil region are in the same direction as the field in the yoke. In the present design, with the coils around the yoke, all of the external fields are in the opposite direction to the field in the yoke. Hence, in the standard C-magnet the fields produced by the end pieces of coil, which are omitted in the 2-dimensional calculation, actually help produce useful field and serve to reduce saturation effects.

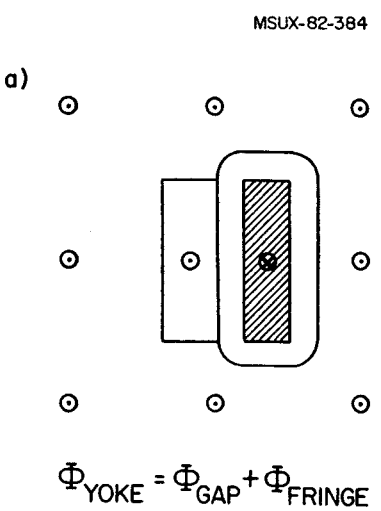

Fig. 4. (a) Schematic comparison of the median plane fields of this C-magnet. In each case the shaded area represents the return yoke.

On the other hand, the end pieces of coil in the present design contribute to saturation of the yoke without adding useful field in the pole tip area. In Fig. 5 are presented Hall probe field measurements in the median plane

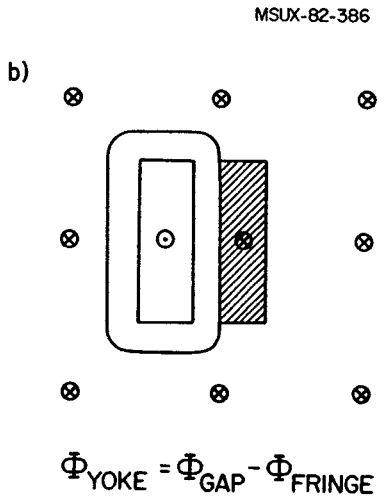

Fig. 4. (b) A conventional C-magnet showing the qualitative difference in the fringing field regions of the two designs.

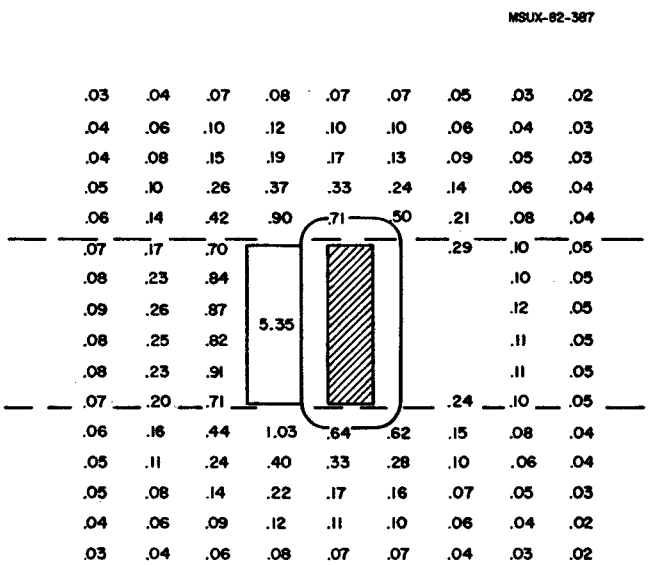

Fig. 5. Magnetic field measurements surrounding the C-magnet. The fringing fields above and below the two dashed lines are not included in the two dimensional POISSON calculation. All of this "extra" flux must be returned by the return yoke of the C-magnet, and increases the saturation of the yoke considerably.

of the present magnet, which were done in order to estimate more quantitatively the magnitude the end effects. An estimate of the amount of flux not included in the 2-dimensional calculation is 1600kG-cm^2. This is sufficient to account for discrepancy.

Despite this inherent magnetic inefficiency, the present magnet should do the job for which it was built. Our concern for understanding the field discrepancy was primarily for use in future designs of magnets with similar geometrical constraints, as well as to increase our understanding of the limitations of 2-dimensional calculations in the designs of 3-dimensional magnets.

Suitability of High Field Magnets for Beam Lines

L.H. Harwood, H.G. Blosser and J.A. Nolen

Plans for the NSCL Phase II beam lines call for all new magnets to be superconducting. Since this includes the dipoles the initial idea was to use small, high-field (3-5T) dipoles to do beam switching. The magnet was to be run by a single power supply with the result that all current densities had to scale together. Thus a field shaping with multiple, independent coils, as done in the cyclotron magnets, was not possible. A simple coil geometry was also necessary in order to keep winding as simple and quick as possible. A "cos θ " dipole was therefore not considered. Design studies were done with the results discussed below. (Note: All calculations were done in two dimensions for an infinitely long magnet.)

The field at some point, B(r), is the sum of two terms, $\mu_o H(r)$ and $B_m(r)$. $\mu_o H(r)$ is the field due to the current distribution and $B_m(r)$ is due to the iron in the problem. If we assume that the iron is saturated, then $B_m(r)$ is a constant independent of the amount of current. $\mu_o H(r)$ is directly proportional to the current. In order to bend beams at all the energies available from the Phase II accelerators, the beam-line dipoles need a dynamic range of about a factor of 2 with 2.5 - 5.0 T as the most likely range of operation. The iron in such a magnet would be fully saturated at all field levels. This means that any change in the central field comes solely from the $\mu_o H(r)$ term. Therefore, if a certain uniformity is desired at different field intensities, then $\mu_o H(r)$ must have that uniformity without the iron. Calculation now becomes trivial because we can solve the linear problem analytically.

The desired region of 10^{-3} uniformity was 2" x 6" (full gap x full width). This was attained by putting the center of the coil approximately 10" from the centerline and 2.6" from the median plane, with the top of the coil 10.6" from the median plane. Field uniformity was about 2×10^{-4} over the desired area. The dimensions of the solution found can be scaled directly if a different size of the uniform region is desired. For example, if a 12" wide region of uniformity is desired, then the above dimensions should be doubled.

With the current distribution determined, the iron configuration is now to be determined. Saturated iron can be simply included into the problem as current sheets placed at the air-iron interfaces. The current density is given by $\vec{B} \times \vec{n}/\mu_o$ where $\vec{n}$ is a unit vector normal to the surface. We have already found the optimum current distribution, therefore the current-sheet model of the iron should have the same geometry, i.e. surface current sheets which replace the saturated iron should have the above solenoid geometry. An analytic approximation to this geometry could not be found, however, because of the nonuniform field in the vicinity of the coil.

Attempts were also made to find a satisfactory configuration using over-relaxation methods to directly calculate the field. The current-sheet model predictions were first checked and confirmed. Several quite different iron configurations were tried, but none were even as good as the zero-order shape predicted by the current sheet model. At any given central field level it was possible to achieve a satisfactory field by shaping the iron; however, any given solution was not satisfactory at any field other than the one at which it was optimized. The conclusion was reached that iron "pole-tips" were not useful since they: a) hurt field uniformity and b) contributed only a small portion of the field intensity.

An iron-free magnet was next investigated. The primary problem found with it was the extended fringe field. 50 inches from the center of the magnet, the field was still 12% of the central field (eg 6 kG with a central field of 50 kG). A double shell of shielding iron was added which had a total thickness of 10 inches. This reduced the field at 50 inches to about 5-8% of the central field, which is still quite sizeable. Addition of the iron also decreased the central field's uniformity even though it was placed far from the region of interest.

The idea of using high field magnets on the beam line was predicted by the desire for small, light magnets which were, hopefully, easy to build. It was found that the desired uniformity and dynamic range for the field was only possible in a nominally iron-free magnet. Such a magnet has undesirably large fringe fields which can only be damped by the addition of large amounts or iron which then reduces the field uniformity but leaves the fringe field at still undesireable levels. The iron also makes the magnet quite massive. It is our conclusion that it is not economical to use a high field magnet, which has only one coil, as a beam line magnet. It appears that a given bend angle is more economically achieved with a longer, smaller-field dipole. Consequently, a study of low field magnets was done. (The results of these studies are reported by Nolen and Zeller.) Other constraints may, of course, make high field magnets indispensible.

A k=1200 ±16° Superconducting Switching Magnet

A.F. Zeller, M.J. Dubois, H. Laumer and J.A. Nolen

Plans for the Phase II beam lines include several superconducting switching magnets, hence economical devices must be designed. Two options we have considered are: 1) small high field magnets where the field profile is dominated by the coil and 2) larger low field (~20 kG), iron-dominated magnets. The high field option has been discarded for reasons reported elsewhere in this annual report by Harwood, et al. This report describes a preliminary consideration of a magnet capable of bending a rigidity of k=1200 through angles of ±16°. Circular cross section magnets, e.g. with cos θ or intersecting circles coil geometries have not been used here because they are quite bulky for large bend angles.

The magnet has a compact trapezoidal shape, as shown in Fig. 1. This results in a magnet weighing only 6500 lbs but with a field uniformity of better than 0.1% in the volume occupied by the beam for fields of 10 to 17.5 kG. The design parameters are listed in Table 1.

Table I. ±16° Magnet Parameters

Pole Width	22 cm (small end) 45 cm (large end)
Gap	5 cm
Iron	6500 lbs
Field Uniformity	±0.1%
Stored energy @ 17.5 kG and operating current	35 kJ
Inductance	7 h

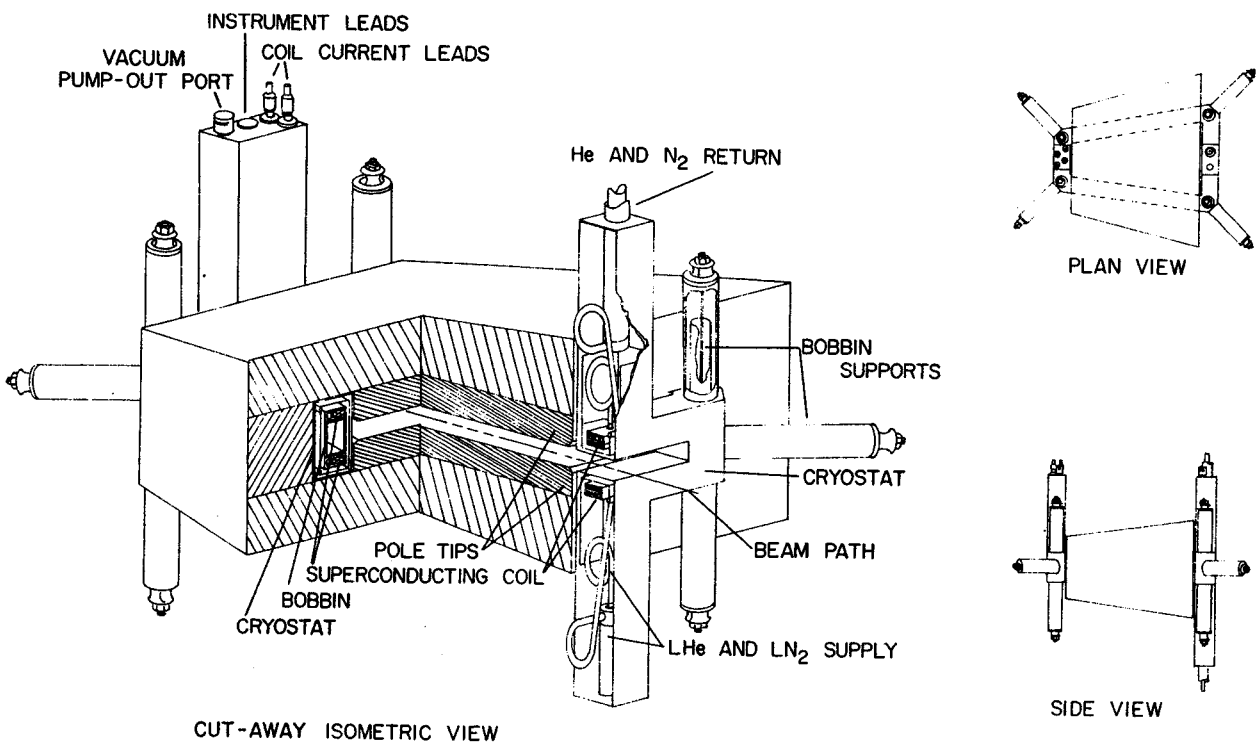

Fig. 1. ±16° trapezoidal magnet.

Since this is a superconducting H-magnet, the problems in coil, bobbin and support structure are similar to those which will be encountered in the S800 dipole magnets, providing a chance to test our design philosophies. It is, however, considerably simplified because there is no negative curvature to worry about and the stored energy is much less than the 1 MJ in the S800.

We are considering a very inexpensive potted coil structure which would not be cryostable. Quench calculations have been performed for this coil design with a quench code from Harwell.[1] Basic wire and coil data for which the calculations were done are listed in Table II. Propagation velocities were taken from those measured by

Table II. Coil Parameters for $\pm 16^{o}$ Magnet.

Packing factor	50%
Turns per coil	500
NbTi Wire (nominal)	
Diameter	0.6 mm
Cu:Sc ratio	5:1
short sample limit @ 2T	170A
Nominal Operating current	100 amps
Ave. Current density	17,000 A/cm^2

Eberhard et al.[2] and Green,[3] and gave qualitative agreement with calculations done using velocities supplied with the code. Shown in Fig. 2-5 are calculations of various parameters as a function of time after the initiation of a normal region at the inner edge of the coil. The solid lines are calculations made without a dump resistor, that is, all the energy ends up in the coil, and the dashed lines are those for connecting a protecting dump resistor as soon as the quench is initiated (the most optimistic possibility).

Fig. 2 shows the decay of the current for a quench at a field strength of 17.5 kG. Fig. 3 shows the growth of the normal zone for both a protected and an unprotected coil assuming a conical propagation. No essential difference between them is observed. Fig. 4 shows the hot spot temperature for both cases, in degrees Kelvin. It is seen that the protected case results in only a slightly lower final temperature, as would be expected since the dump resistor takes away only a few kilojoules, because the quench propagates so rapidly. Fig. 5 shows the internal resistive voltage as would be found if, for example, the top half went normal while the bottom coil remained superconducting. Half of this voltage would show up across each coil. The protected case results in approximately 50 volts lower potential than the unprotected. Since the insulation must withstand over 600 V in either

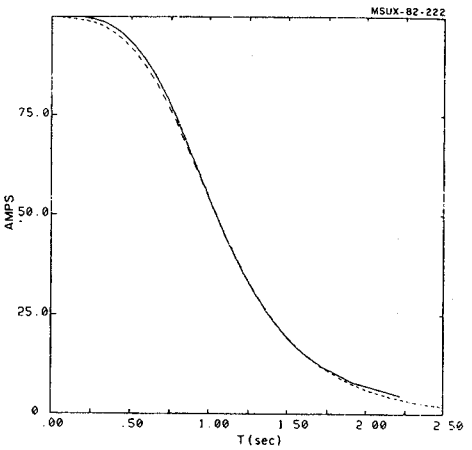

Fig. 2. Decay of the current in the coil with a dump resistor (dashed line) and without a dump resistor (solid line) during a quench.

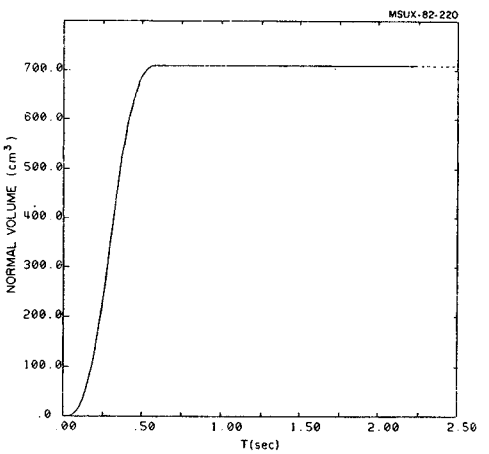

Fig. 3. Growth of normal zone in the coil.

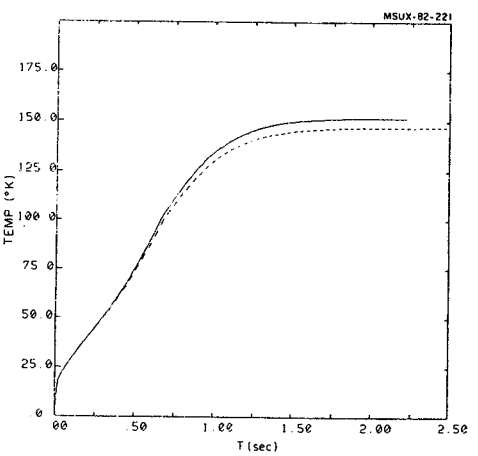

Fig. 4. Hot spot temperature in the coil.

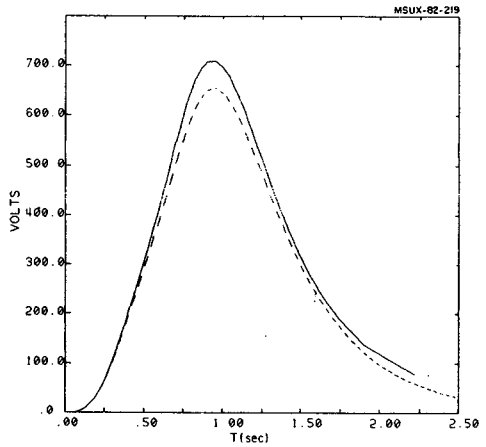

Fig. 5. Internal voltage in the coil.

case, the protection resistor offers only marginal advantages. It was decided, therefore, to eliminate the expensive protection circuit since the calculations show that the coil should survive a quench. Detailed design of the coil structure and the mechanical design of the bobbin and cryostat are in progress. Construction of a prototype magnet should begin this Winter.

---

1. M.N. Wilson, Harwell Library (unpublished) 1971.
2. P.H. Eberhard, et al., LBL Report 12337 (unpublished) 1981.
3. M.A. Green, LBL Report (unpublished) 1981.

Quenching of Superconducting Magnets by Nuclear Radiation Heating

J.A. Nolen, Jr.

The phase II beam transport system and several experimental devices will utilize magnets with superconducting coils. For magnets with little stored energy, it is common use epoxy-potted coils in such magnets. Tests at Fermi Lab have shown that a single pulse of nuclear radiation as little as 1 mJ/g can quench such magnets. This is due to the lack of intimate contact between the conductor and liquid helium in potted coils, as well as the very low specific heat of the coil composite at liquid helium temperature (~1mJ/cm^3-K). In cryostable coils, such as in the K500 and K800 cyclotrons, the conductor is in direct contact with liquid helium which can easily dissipate such radiation energy doses because of its high latent heat of vaporization (~20 J/g).

It is shown below that whereas radiation energy doses far exceeding 1 mJ/g may often occur in the NSCL beam line magnets, the time constants are such that this energy can be dissipated by thermal conductivity through the coil composite to the liquid helium before the magnet quenches. The Fermi Lab tests involved relatively small energy deposits (1 mJ/g ~ 100 Rad. dose) given in very short pulses (20 μ sec). The neutron shielding report of Naryanaswamy, et al (MSUCP-40-1982) for NSCL phase II shows that in certain locations near unshielded beam dumps neutron radiation levels as high as 10^6 rad/hr may be encountered for short periods of time. This corresponds to an absorbed energy of about 3 mJ/g per second. However, a continuous energy deposit at the rate of 3 mJ/g per second will generally not quench a magnet, even though a short pulse of 1 mJ/g can do so.

First we will consider the equilibrium temperature distribution within a semi-infinite coil composite cooled at the surfaces by liquid helium and heated internally by neutron and/or gamma radiation. Then we will consider the time constant (τ) for the transient response during which the temperature profile changes from a constant 4.2°K prior to the onset of the radiation dose to the equilibrium profile of the steady state solution. Obviously, for very short pulses it is the total energy per unit mass and the specific heats (c) which determine the temperature rise, whereas for steady state radiation it is the rate of energy deposit per unit mass and the thermal conductivities (k) which determine the temperature rise. For intermediate length pulses (times ~ τ) it is the ratio k/c which determines the response.

Consider the geometry depicted in Fig. 1. The coil of thickness a cm is subjected to uniform dose rate R mJ-g^{-1}-sec^{-1} (per unit mass) or D=Rρ mJ-cm^{-3}-sec^{-1} (per unit volume). The dose rate is such that it is easily dissipated by the helium bath at 4.2 K. The equilibrium temperature profile is indicated schematically in the Fig. It arises from integrating the heat flux equation:

MSUX-82-393

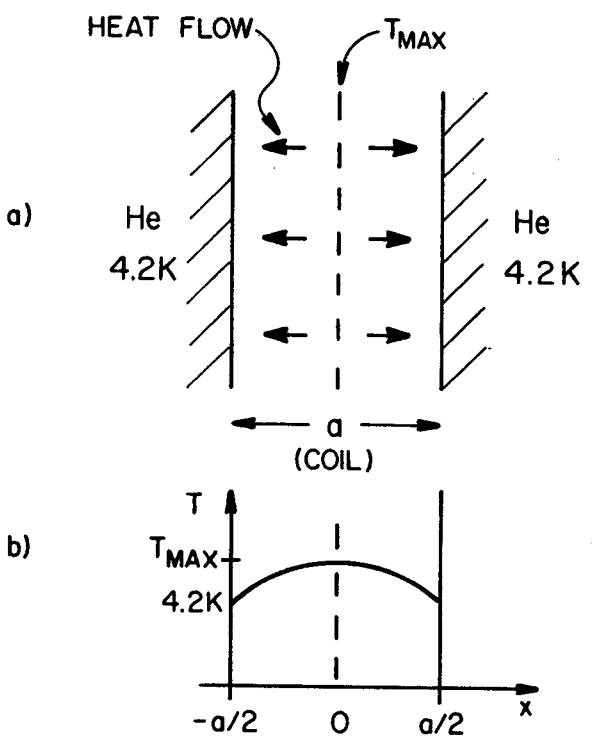

Fig. 1. a) Schematic section of a semi-infinite coil composite of thickness "a" cooled at the surfaces by liquid helium at 4.2K. Neutron or gamma radiation deposits energy within the coil which will flow from the interior to the helium bath as indicated. b) The corresponding one-dimensional temperature profile at equilibrium.

$$\Phi = - k \frac{dT}{dx} \quad \text{mJ-cm}^{-2}\text{-sec}^{-1}.$$

This gives the temperature rise at the coil center at equilibrium:

$$\Delta T = \frac{R\rho}{k} \int_0^{a/2} x \, dx$$

$$= \frac{R\rho}{k} \quad \frac{a^2}{8}$$

We will express the answer for three cases in terms of the energy or radiation flux rate required to raise the central temperature of such a coil 1° K.

a) Pure copper coil $\rho \simeq 8$ g/cm^3, k $\simeq$ 1000 mJ-sec^{-1}-cm^{-1}-K^{-1}, ΔT=1K, a=1cm, yields R=1000 mJ-g^{-1}-sec^{-1} = 360 x 10^6 Rad/hr.

b) Typical epoxy fiberglass composite Same as a), except $\rho \simeq 3$ g/cm^3 and $k \simeq 1$ mJ-sec^{-1}-cm^{-1}-K^{-1}, $R \simeq 3$ mJ-g^{-1}-sec^{-1}=10^6Rad/hr.

c) Typical potted coil (cut epoxy fiberglass) Same as a), except $\rho \simeq 6$ g/cm^3 and $k \simeq 10$ mJ-sec^{-1}-cm^{-1}-K^{-1}. $R \simeq 13$ mJ-g^{-1}-sec^{-1}=5×10^6 Rad/hr.

Cases a) and b) are intended to represent extremes and case c) a representative potted coil composite. (Data are from S.L. Wipf, Los Alamos report LA-7275, 1978). Note that the tolerable dose rates scale inversely as the square of the coil thickness a. Note also that the tolerable dose rate for steady state situation depends linearly on the difference T_c-T, where T_c is the critical temperature and T is the normal operating temperature (e.g. 4.2K). A coil operated at $I/I_{max} = 0.5$ can tolerate 5 times as much radiation dose as a coil operated at $I/I_{max} = 0.9$, etc.

Detailed consideration of the temperature profile during the transient period following the onset of a setup function of radiation dose involves the inhomogeneous diffusion equation:

$$D + \left(k \frac{d^2T}{dx^2}\right) = c\rho \frac{dT}{dt}$$

where D is the energy dose rate per unit volume, and T(x,t) is the transient temperature profile. We are primarily interested in the temperature at x=0 where it is always at its maximum value. Hence we postulate a solution for T(0,t) of the form:

$$T(o,t) = T(o,\infty)\ [1-\exp(-t/\tau)]$$

where $T(o,\infty)$ is the equilibrium solution and τ is the time constant for the transient response. Pluging the trial solution into the diffusion equation for x=o we obtain an expression for the time constant:

$$\tau = \frac{c\rho a^2}{8\ k} \text{ sec.}$$

A rough estimate of this time constant is given by again assuming a=1 cm, $c\rho \simeq 1$ mJ-cm^{-3}-K^{-1} (for either pure Cu or a coil composite), and $k \simeq 10$ mJ-sec^{-1}-cm^{-1}-K^{-1} for coil composite or 1000 mJ-sec^{-1}-cm^{-1}-K^{-1} for pure copper. This gives a range of time constants:

$$0.12 \text{ msec} < \tau < 12 \text{ msec}$$
(pure copper) (coil composite)

In either case we see that $\tau \ll 1$ sec and the equilibrium solution can be used for the purposes of the present consideration for NSCL. These short time constants do permit a consistent explanation of the difference between the Fermilab tests with 25 μsec pulses and the present estimates of steady state radiation tolerance.

The above mentioned radiation levels can be locally much larger if direct charged particle beams penetrate into the coil. Such penetrations should be prevented by shielding the cryostat from the direct beam. There can also be additional heating if the coil composite contains certain elements such as boron which have abnormally large neutron capture cross sections.

Design Studies of the K500 to K800 Transfer Beamline

L.H. Harwood, J.A. Nolen and H.G. Blosser

A preliminary design study for the beam transfer line between the K-500 and K-800 cyclotrons under construction at the National Superconducting Cyclotron Laboratory (NSCL) was carried out in 1979 and reported upon.[1] Positioning of the two cyclotrons relative to each other was decided based on the results of that study. A preliminary design for an achromatic coupling line was presented and studies of a system which was both achromatic and isochronous were initiated. Since that time, new beam extraction calculations have been done for the K-500 cyclotron with some significant changes in some beam phase space ellipses. There have also been changes in the characteristics of the injected beams for the K-800, due primarily to the major redesign of the pole tip shapes. The physical layout of the transfer line has been somewhat restricted by installation of major items in the high bay, specifically the liquid helium plant has been installed in the high bay south of the K-500. The west highbay region is shown in Fig. 1.

The present calculations are continuations of the earlier studies with the new constraints mentioned above. In these calculations only solutions which are both achromatic and isochronous are being considered. The purpose of the following report is to describe the current status of the transfer line calculations. This report will describe the conceptual design.

The overall requirements for the transfer line are: 1) to get the beam from one cyclotron to the other, 2) maintain the pulse length (i.e. the complete coupling line will itself be isochronous), 3) have an achromatic double waist somewhere near its midpoint (i.e. a point where the beam has specified radial and axial sizes and no linear or angular dispersion in order to decouple the tuning of the K500 from that of the K800), and 4) match the phase space ellipses (including dispersion) of the beam extracted from the K500 to the acceptance ellipses of the injection channel of the K800 cyclotron. An auxiliary detail that must be addressed pertains to laboratory scheduling: for maximum flexibility, the K500 cyclotron should be able to provide beam for experiments in a stand-alone mode as well as being an injector for the K-800 cyclotron. This, however, is not paramount in the considerations. A minimum system can be specified by applying the above requirements in turn. Some of them will be easy to fulfill, others more difficult.

I) Tuning Simplicity

Tuning the elements of the transfer line is a delicate task, and any help that can be provided to the cyclotron operators by the optical design will be quite useful. We have chosen to have the transfer line divided into two major sections; the first section will end with an achromatic double

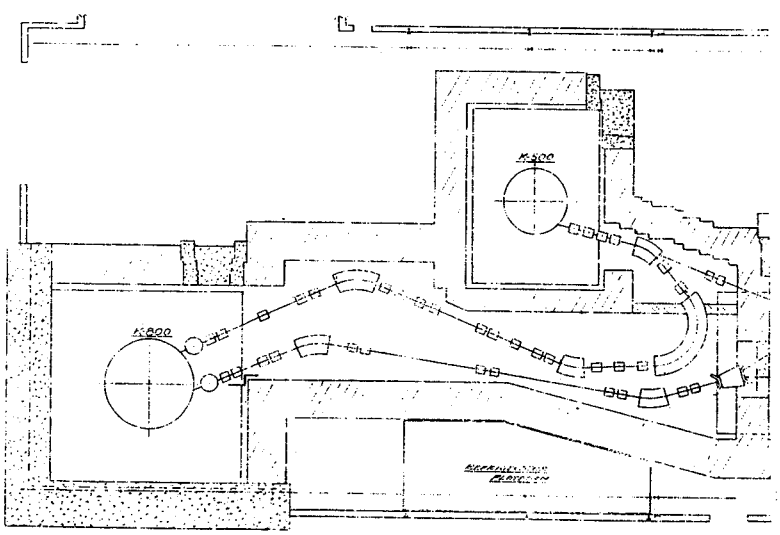

Fig. 1. Plan view of NSCL Phase II West High Bay (Quadrupoles are represented by rectangles on beam line.)

waist of a specified size and will make the entire transfer line isochronous. The second section will emittance and dispersion match this waist into the acceptance of the K800 injection channel. The optical design and proper tuning are simplified by this choice: the design is broken into two nominally independent parts, and a good tune for the first section of the system can be achieved independent of the tuning of the second section.

II) Connecting the Two Cyclotrons and Isochronism

The most obvious element that is needed in the system is a large dipole (bend angle= 180 deg) to turn the beam toward the K-800. This large bend is also essential to isochronize the transfer line since the pulse length term (for non-monoenergetic rays) is $L-\int d_x da$ (where L=length of system, d_x= linear dispersion, and da is an incremental angle of bend in a dipole); thus, if the bend angle is large, then the pulse length term can easily be made large. For a bend angle of 180 deg and L=30 m, we need d_x to have an average value of 10 cm/%. This in itself is not a difficult condition to fulfill; however, fulfilling it simultaneously with the other conditions may well be. We will, at the very least, require a quadrupole before the large dipole to adjust the wide range of values of d_x that the extracted beams will have. The resulting simple system is shown in Fig. IIa.

III) Scheduling and Achromaticity

In order to minimize interference with the research program with the K-500, a small dipole is needed early in the system to switch the beam between the experimental beam lines and the transfer line. With this provision the K-500 can operate in stand-alone or injector mode with minimal switching problems.

A third dipole is convenient in tuning the beam to be achromatic at the double waist. Strictly speaking, this dipole is not needed. If one assumes that quadrupoles can adjust d_x and d_x', to any desired values, then it is possible to make the system isochronous and achromatic with the two previously mentioned dipoles. Unfortunately, after solving the equations one finds that the large dipole would need a bend radius of about 17 m to accomplish this feat and would still have the large bend angle needed to send the beam toward the K-800 thereby occupying a large amount of floor space. The easier solution is to maintain a reasonable field (10 - 20 kG) in the large dipole and to add quadrupoles and the third dipole. We still need to control d_x and d_x' at the entrance of the large dipole and thus need quadrupoles between the first two dipoles. The two optical conditions at each dipole require at least two quadrupoles before each dipole. For optimum effect, one quadrupole should be very close to the entrance of each dipole and one should be far away. All of the above requirements are met by the schematic system shown in Fig. 2b.

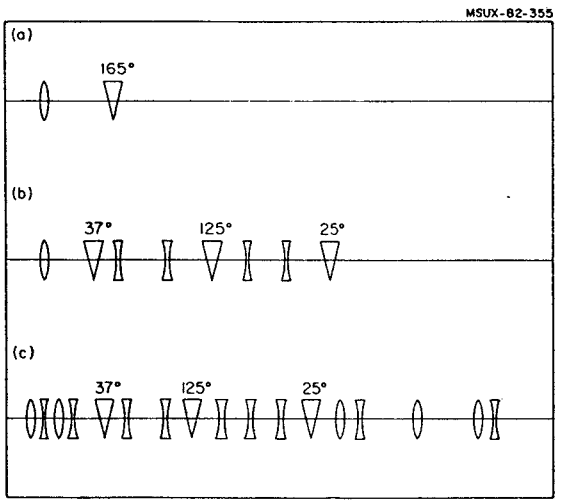

Fig. 2. Illustration of conceptual design of first half of coupling line. Convex lens shapes are x-focusing quadrupoles, concave shapes are y-focusing quadrupoles, and triangles are dipoles with their bend angles given above the triangles.

IV) Emittance Matching

The phase space ellipses of various beams extracted from the K-500 are not constant; neither are the ones accepted by the K-800. We have already partially addressed the problem of the variations by separating the transfer line into two parts which meet at an achromatic double waist. The first section needs additional elements to make this possible. d_x for the extracted beam ranges from +2 cm/% to -15 cm/%. The system we have specified so far could not accommodate this range. Therefore, we add three quadrupoles at the beginning of the system.

We have yet to provide the elements to form the double waist at the end of the first section. An infinite variety of quadrupole arrangements could work, but mathematically we only need two quadrupoles to get the double waist condition. We stated above that the beam would have a specified size, therefore we need at least two more parameters (i.e. quadrupoles) to control the waists' sizes. Another doublet or a triplet

would work. For maximum flexibility we have chosen a singlet followed by a doublet; this keeps the beam size reasonable in the beam tube and keeps the quadrupole gradient reasonable. The resulting system is shown in Fig. 2c.

V) Additional Considerations

The earlier study used a high-field (B=38 kG) dipole for the "switching" magnet. The high-field beam line magnet study (see separate report) indicated that such magnets were not well suited to beam lines. A longer, lower-field magnet was deemed more feasible, so it replaced the high-field magnet in the present study.

VI) Present Status

The present system appears promising. Drift lengths and dipole lengths have changed small amounts from the earlier study, and the sign of the exit edge angle on the large dipole has changed. The only additions of a components are quadrupoles before the first dipole and between the second and third dipoles. The envelope sizes are reasonable everywhere as are the quadrupole gradients. The setup of the system looks straightforward, too. One can start with approximate quadrupole settings and quickly get a calculated solution. The solutions appear to be relatively easy to adjust for slight errors in field settings as these errors tend to cause the beam to blow up at measureable locations.

The studies of the first section has been completed for all beams. Initial calculations of the K800 injection matching section have been done, as has a schematic design of the line to transport the beam to the experimental areas from the K800. The results of the above work is shown in Fig. 1. The final calculations must await the final injection and extraction studies of the K800 (which are in progress).

K500 Ion Source and Associated Systems

T.A. Antaya, M.L. Mallory

The 1976 proposal for the K500 Cyclotron called for dual PIG sources, remotely insertable thru locks in the pole centers. In this way, a spent source could be retracted, and a fresh source, waiting in the other lock, inserted and struck without shutting down the cyclotron to make the change. With the achievement of several milestones in the past year, we are now not far from realizing that goal.

Many cyclotron sub-systems, like the extraction elements, beam probe and ion sources were programmed into the last stages of the cyclotron construction phase. As a result, work did not begin on the ion sources until after the rf resonators were well along. The 7 inch diameter center plugs, containing the zero trim coil, central region defining surfaces, and the ion source vacuum locks, were assembled in August 1981 and installed in the cyclotron in early September. At this time fabrication of parts for the lower PIG source was also well under way. Initial operation and testing of the lower source began in early October 1981, using the de-commissioned K50 cyclotron as an ion source test stand. This allowed the ion source testing to be performed in parallel with the initial testing of the 3-phase rf-system in the K500 cyclotron. Several modifications were made in the source design and operation, culminating in a sustained high arc power run of 9 hours on 31 October 1981. The source was then moved to the K500, and has since been employed exclusively for beam tests.

The overall compactness of the central region of a superconducting cyclotron is evident in Fig. 1. The ion source extraction slit resides off center in a 2 inch diameter hole in the center plug. The center plug is an intricate device, with many functions in addition to providing the air lock and axial alignment for the ion source. The copper cap completes the beam chamber vacuum wall, the rf liner surface, and covers the iron tips of the pole pieces. This iron used to shapes the central magnetic field for the initial ion acceleration. A circular trim coil is mounted within the center plug. We will change the central region with each harmonic, by modifying removeable dee tips thru the center plug.

We have chosen an all manual gas manifold design for gas supply, as shown in Fig. 2. The manifold resides inside a vented hood for containment of toxic gases. Two separate inlet sections, with independent servo-controlled gas flow, and joined on the low pressure side of the needle valves, are provided for source gas mixing. The choice of components and materials has at present limited us to non-corrosive gases. The gas manifold is outside the cyclotron vault, approximately 11 m. from the cyclotron.

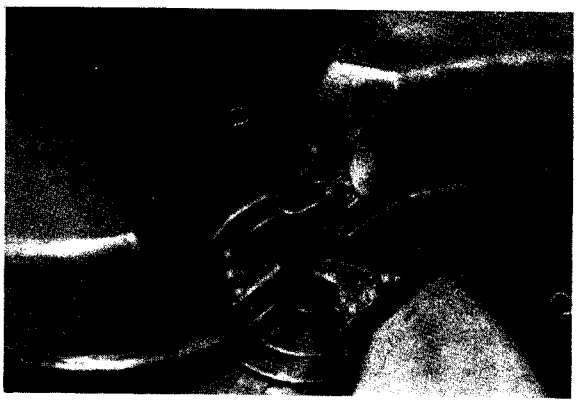

Fig. 1. The overall compactness of the central region of the K500 is evident in this photograph. The lower ion source resides between the three dees near the center. The edge of the lower center plug is visible in the valleys and the mounting screws for the dee tips can also be seen.

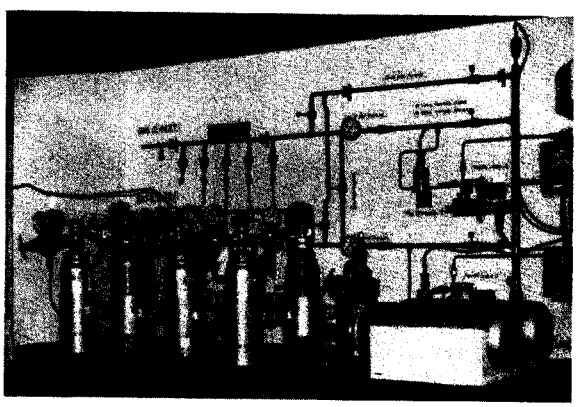

Fig. 2. The gas manifold is installed in a vented hood outside the cyclotron vault. The inlet section is to the left and the needle valve servo units and flow meters in the right side of the hood. The flow control modules are located at the control console.

The lower PIG source design is shown in Fig. 3. (The upper PIG source, under construction now, is a mirror image of the lower about the median plane.) This source contains no iron, to allow removal from the cyclotron with the main magnet on. The high voltage vacuum feed thru is at the external end of the source. Protection of the alumina insulator requires high vacuum pumping of the space in which the ion source resides, currently via a small diffusion pump, but eventually by a cleaner means. The source design has been quite amendible to re-

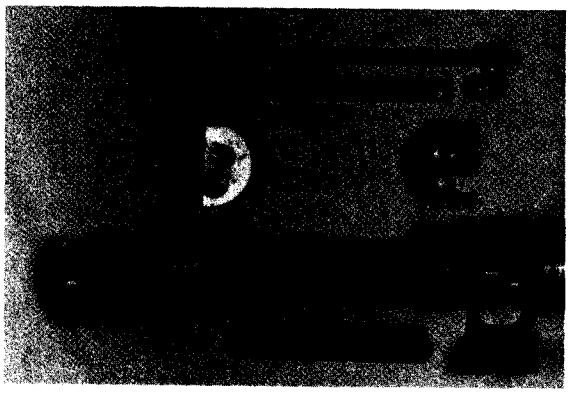

Fig. 3. The photograph shows the lower ion source assembly and principle elements of the arc in exploded view. Cathodes are mounted off a waxially water-cooled copper high voltage rod on small tantalum holders. The chimney is formed by folding .050 inch tantalum sheet stock over a form and TIG fusing the seam in an inert gas chamber. In this way the chimney stays remaining and a slit can be machined. Small expendible copper transitions align the chimney and define the arc gap. All other indirectly cooled arc parts are made out of tantalum. Gas is fed into one end of the chimney.

cycling, with a cycle time of approximately 25 minutes from spent source to fresh source back in the cyclotron. The main contribution to the cycle time comes from the lock pump down and re-insertion of the source.

To date, we have logged about 115 hours of operating time on the lower source, during 57 runs of which 49 were beam tests, in which the source was responsible for terminating the beam test only 25% of the time - thru cathode wear mainly or other source failures. As we gain more experience with this source, several abnormal failure modes have been identified, and we have been successful in eliminating most of these thru design or operation changes. The last 50 hours of operation have been without failure. Daily operation has become quite routine. Operation in the high field magnet has brought on a few differences in the operating characteristics. The source appears to run with lower gas flow in the high magnetic field. Due to the median plane restrictions on the size of the ion source cross-section, water cooling lines are small and the ion source runs hot. The source lifetime for medium weight ions (C,N,O) looks to be in excess of 6 hours at two kilowatts of arc power. During the beam tests we have principally operated the source on CO_2 or CO_2+ deuterium (for deuterium beams), though CO, N_2 and N_2+H_2 have also been tried. Typical performance data are shown in Fig. 4. This data exhibits characteristically PIG behavior.

We have the facilities for the supply of a large number of gases to the source, and as

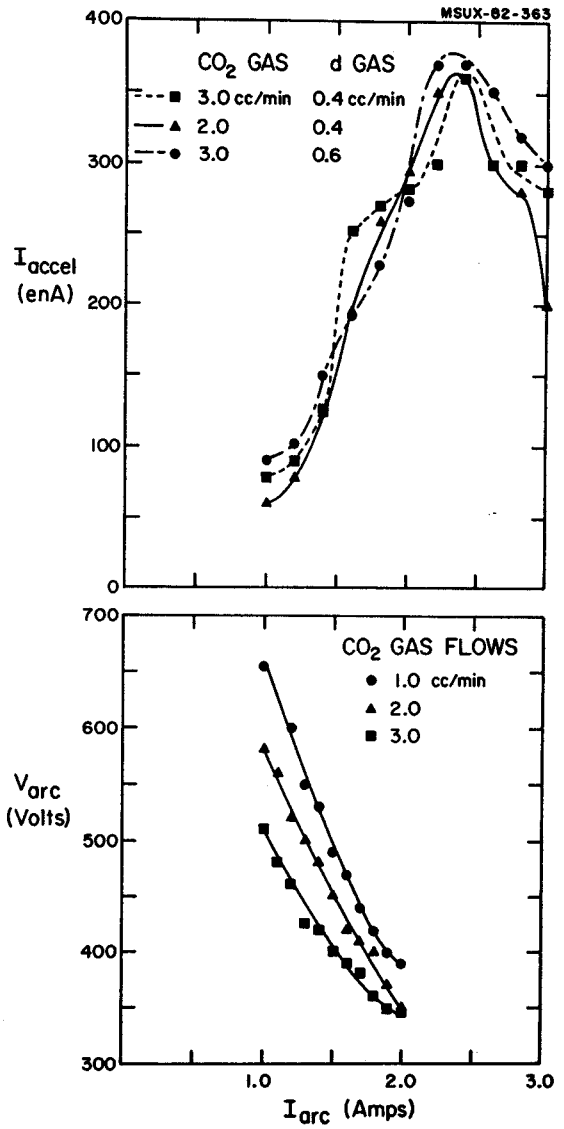

Fig. 4. Characteristic arc parameters taken during the development of early carbon and deuterium beams. The upper graph shows data for 53 MeV/A deuterium accelerated to full radius with CO as the arc support gas. An arc current of 2.3A appears to be optimum. In the lower graph the variation of arc voltage with arc current and gas flow is shown. The ability of the source to maintain the arc with low gas flows (1.0 cc/min) was very valuable during the cyclotron commissioning.

the cyclotron moves into its first operating cycle to begin looking in detail at the source performance characteristics. To complete the system, we await the fabrication of the upper source, now about 40% complete, and the drive units to automatically insert the sources thru the locks, now in the design stage.

Canonical Treatment of Accelerated Orbits and a Proper Phase Definition

M. M. Gordon

As noted in last year's report, we have been concerned with improving the analysis of accelerated orbits in cyclotrons in order to understand more completely various coupling effects associated with the acceleration process. One paper[1] dealing with radial-longitudinal coupling effects has already been published and, in the meantime, we have been working toward generalizing the analysis and incorporating some of the results into our orbit computation programs.

Unlike Schulte and Hagedoorn,[2] our analysis is based on a completely relativistic hamiltonian and formulated in standard polar coordinates (r,θ,z). As is customary, we change independent variables from t to θ using a relativistic form of Hamilton's principle. We then find that in addition to the canonical pairs (r,p_r) and (z,p_z), we now have the pair (t,p_t), where $p_t = -H$, and $H = E + q\phi$ is the usual hamiltonian.

In addition, the canonical angular momentum p_θ becomes (with a sign change) the new hamiltonian: $K = -p_\theta$, where now, $K = K(r,p_r,z,p_z,t,p_t;\theta)$. As usual, the canonical momenta p_r, p_θ, and p_z include the contribution from the corresponding components of the vector potential $\vec{A}$.

Instead of H, we prefer to have the ion's kinetic energy E itself as one of the variables, and we therefore use a gauge transformation to change the set of potentials from $(\vec{A},\phi)$ to a new set $(\vec{A}',\phi')$ such that $\phi' = 0$. In this case, we obtain:

$$\vec{A}' = \vec{A} + c \int (\nabla\phi)dt, \qquad (1)$$

and this choice of vector potential is also a very suitable representation for RF fields (as well as static magnetic fields).

For the given median plane magnetic field, we assume that all equilibrium orbit (e.o.) properties are given as a function of E. Such information is readily available, for example, from a standard e.o. code, and it is quite customary to store such data for reference purposes within programs designed to calculate accelerated orbits.

The coordinates specifying the e.o. as a function of E and θ are represented by the following functions: $r_{eo}=R(E,\theta)$, $(p_r)_{eo}=Q(E,\theta)$, and $t_{eo}=(\theta/\omega)+\psi(E,\theta)+u$, where as usual, $\omega=2\pi/\tau$, and where R, Q, and ψ are all periodic functions of θ. This ψ results from the noncircularity of the e.o., and u is simply a constant specifying the "starting time".

As usual, in characterizing some other orbit, we use: $x=r-R(E,\theta)$, and $p_x=p_r-Q(E,\theta)$, so that (x,p_x) gives the radial displacement from the e.o. at each E and θ. If this change is carried out with a canonical transformation which leaves E invariant, then we find that t is replaced by a new variable u given by:

$$u = t - (\theta/\omega) - \psi + (\frac{\partial R}{\partial E})\, p_x - (\frac{\partial Q}{\partial E})\, x, \qquad (2)$$

assuming that for motion in the e.o. (with $x=p_x=0$), this u reduces to the starting time defined above.

What seems most interesting is that our analysis shows the coordinate u to be a constant of the motion for any non-accelerated orbit executing strictly linear oscillations about the e.o., and moreover, this is true not only for cyclotrons but for any FFAG accelerator. This conclusion follows from the fact that an expansion of the hamiltonian contains no first order terms in x and p_x (or z and p_z) in the absence of acceleration.

Consider, for example, the usual 2 x 2 transfer matrix which carries the vector (x,p_x) from one gap crossing to the next at a fixed energy E. Since u is also constant for this orbit segment, the change in the time t can be calculated directly from the above eq. (2) relating t and u. That is, we need not enlarge the transfer matrix to find time changes between gap crossings.

The coordinate u also leads quite naturally to a proper definition of the phase which characterizes the average rate of energy gain for an accelerated orbit. As noted before,[1] ϕ should be defined so that it is a constant of the motion for a mono-energetic group of ions executing linear oscillations. Since u is just such a constant, we should set $\phi=\omega_{rf}u = h\omega_o u$, where ω_{rf} is the RF angular frequency and h its integral harmonic number.

This ϕ definition is exactly correct only for an isochronous field where $\omega=\omega_o$ independent of E, but it requires only a minor change for any field of practical interest.

This ϕ definition is also completely consistent with the one previously obtained for circular orbits. In this special case, both $\psi = 0$ and $Q = 0$, and R is constant. In addition, $\partial R/\partial E = R/vp\nu_r^2$, and we then have:

$$\phi = \omega_{rf}t - h\theta + hp_x/p\nu_r^2,$$

which is exactly our old result.

Another byproduct of this analysis is that it leads directly to Joho's hamiltonian.[3] That is, if we extract the part of our hamiltonian which depends only on E and u (or ϕ), and then through averaging, consider only the secular variation, we obtain Joho's hamiltonian, which is not only an invariant, but which displays the phenomenon of phase compression.

Because the action integrals associated with the linear oscillations are important adiabatic invariants, we are also considering canonical transformations to angle-action variables. Although this work is still in progress, one immediate result is that such a transformation again alters the phase definition by adding terms which are quadratic in the oscillation amplitudes.

1. M.M. Gordon and Felix Marti, Particle Accel. 12, 13 (1982).
2. W.M. Schulte and H.L. Hagedoorn, Nucl. Instr. and Meth. 171, 409 (1980).
3. W. Joho, Particle Accel. 6, 41 (1974).

Cryosystems

M.L. Mallory, H. Laumer, A. Gavalya

The following sections are a summary of progress with various cryogenic systems during the past year and previous annual reports should be referred to for additional information.

K500 Cryostat

We have previously reported a method for finding leaks in the helium cryostat with liquid helium. We have now found and fixed all leaks in the K500 cryostat and are able to operate the cryostat vacuum jacket with no external pumping (for at least 6 months). We have detected some unusual phenomena with the cryostat vacuum system during cooldown. The vacuum jacket is pumped on with a small diffusion pump which achieves 10 micron at room temperature. At 250K where water is completely frozen out, a large improvement in the vacuum is detected and it continues to gradually get better as the cryostat cools. At 40K, where nitrogen gas is frozen out, the vacuum observed is in the 10^{-6} Torr range, however it then gets worse (up to 10^{-5} Torr). We find that closing off the diffusion pump allows the vacuum jacket to improve (down to the 10^{-7} Torr range). It appears to us that the diffusion pump system is now a vacuum leak and it would have to be helium gas for it not to be cryopumped.

K500 Refrigerator

The refrigerator for the K500 is a CTI 1400 with three compressors. Two modifications have been made that have significantly improved the down time. We installed new tappered bearings in the engine piston connecting rod. These bearings allow for greater misalignment then the previous bearings and have greatly extended the lifetime between change. Secondly, the valve rod "O" ring seals have been replaced with hydraulic type seals that have greater wear capabilities. Our biggest maintenance problem is to time the replacement of the charcoal beds of the oil compressors before bleed through, while keeping the system operational. If bleed through does occur, we can warm up the warm end of the heat exchangers in a few hours and completely recover the helium system within one day.

K500 Cryolines

The need to simultaneously feed liquid helium to the K500 magnet and independently to the cryopanels located inside the cyclotron dees has required the construction and operation of a parallel branch liquid helium distribution system. In addition, a parallel branch liquid nitrogen distribution system, coaxial with the liquid helium system, that reduces the helium heat load, has also been constructed. Fig. 1 and 2 are simple line drawings of the liquid nitrogen and liquid helium systems, Fig. 3 is a more realistic line drawing showing the total distribution system as built. The system is now running and some initial results have been obtained.

1. The total heat load of the system is less than the 1400 refrigerator output.

2. The system excess capacity, when feeding only the K500 magnet, is now greater than ever, thereby indicating that the old transfer lines (non nitrogen shielded) were a large fraction of the previous magnet heat load.

3. Vacuum within the acceleration chamber with two of three cryopanels cold and no ion source gas has been measured to be as low as 3 x 10^{-7} Torr.

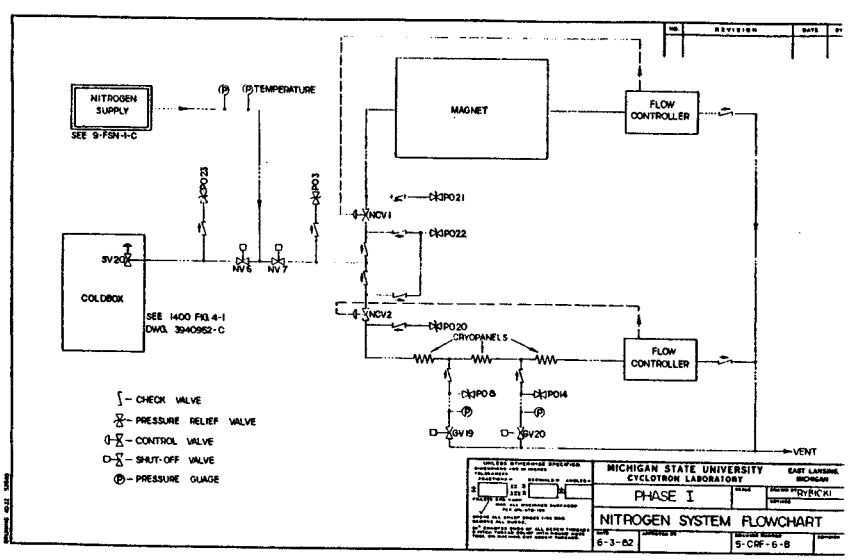

Fig. 1.

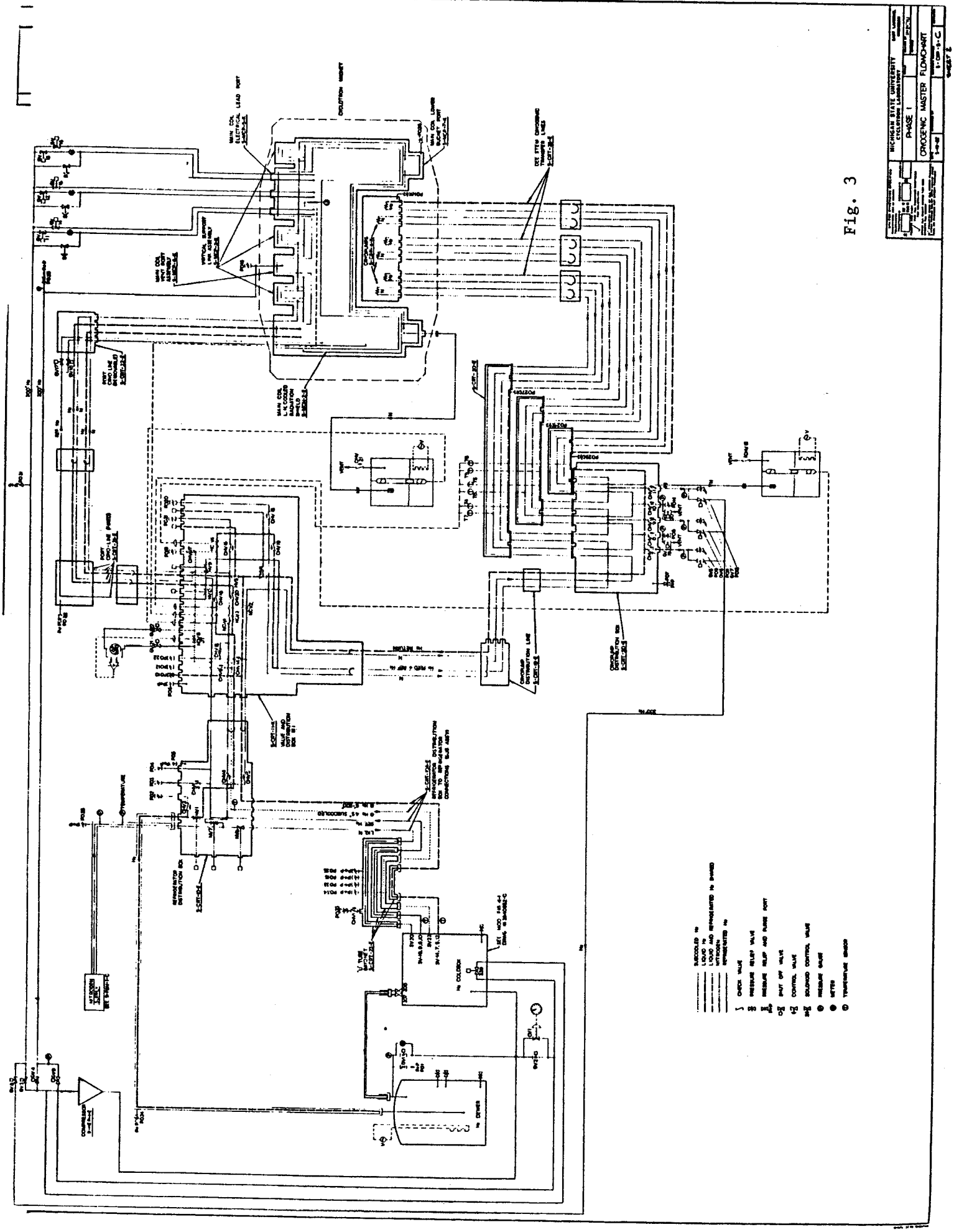
MICHIGAN STATE UNIVERSITY
CYCLOTRON LABORATORY
PHASE I
CRYOGENIC MASTER FLOW CHART
C
SUBCOOLED He
LIQUID He
LIQUID AND REFRIGERATED He MIXED
NITROGEN
REFRIGERATED He
CHECK VALVE
PRESSURE RELIEF VALVE
PRESSURE RELIEF AND PURGE PORT
SHUT OFF VALVE
CONTROL VALVE
SOLENOID CONTROL VALVE
PRESSURE GAUGE
METER
TEMPERATURE SENSOR

Fig. 3

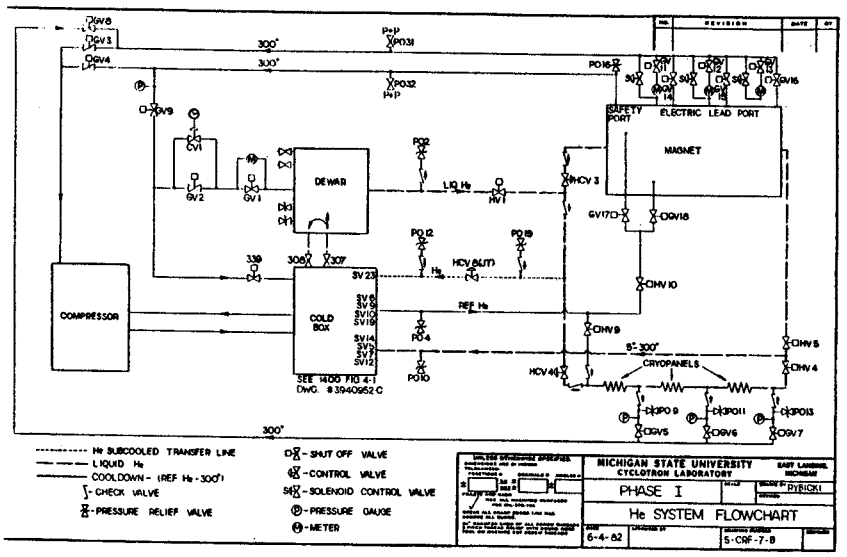

Fig. 2.

4. The system in manual feed seems to run very smoothly in delivering liquid helium to both the magnet and the cryopanels.

Several problems have been encountered. A section of the distribution system has an internal helium leak (box 1) and requires continuous pumping. It will be repaired in the future.

In bringing the cryopanels on line, with cold gas returning from the magnet, a large length of the return line can not be precooled and thereby causes the low temperature end of the cold box to see a huge heat pulse. We are able to control this by valves in the refrigerator, but are planning to add a cooldown line to box 1, when the helium leak is fixed.

One cryopanel developed a helium leak during the first cool down and it will have to be fixed. The seals of the coaxial feed and return helium bayonets to the cryopanel were found to leak, thereby providing a short circuit path for the liquid helium and thereby not cooling the cryopanels. A commercially available stainless steel springloaded teflon seal has been found to seal satisfactorily. In summary, the K500 cryoline system does meet our requirement of operating the cyclotron.

K800 Refrigerator

The major components of the K800 refrigerator were delivered and assembled on site during the past year. Fig. 4 shows the cold box in its operating location. In June the cold box was first operated and cool down proceeded to liquid helium temperature. The run was terminated because of plugged gas thermometers and wrong gas in several of them. In July, the system was again operated and it successfully made liquid helium at the rate of 100 l/hr. The run was terminated after the detection of several problems, the most serious being that the compressor mass flow was only 1/2 of that needed for the performance specification. When the compressor mass flow equals the expected value, the refrigerator will again be tested for its performance specification.

Fig. 4.

A Time Saving Vacuum Leak Checking Technique

H. Laumer, M. Mallory

A large portion of the equipment at the National Superconducting Cyclotron Laboratory relies on chambers that must be leak tight with respect to the surrounding atmosphere. A considerable amount of time is spent to leak proof components or entire chambers. This note discusses a leak checking technique which avoids machining special fittings for the sole purpose of leak checking parts; a substantial saving in cost and time is achieved.

The first obstacle encountered in leak checking a component is usually the lack of a convenient coupling between it and the helium mass spectrometer. For a vacuum test, where in the past test chambers or fittings with elastomer O-ring seals have been machined, a time saving technique employing tape supporting a putty-like sealant to improvise test chambers has been developed. We usually use duct tape[1] and a duct sealing compound[2]. Not all duct sealing compounds work equally well; we have found that some brands outgas more than others and are unsuitable for this application. More expensive compounds, such as Apiezon Q wax, would work as well.

Fig. 1 through 3 illustrate the capability of the technique. Fig. 1 shows one of 3 capacitive couplers which are used between the RF transmission lines and dees of the superconducting cyclotron. The location of a number of weldments are indicated by arrows. For a check of all weldments a setup such as Fig. 2 is employed. It uses a copper tube as a test chamber and vacuum seals are made with tape and sealing compound at one end and with a rubber stopper coupled to a flexible hose at the other end. The flexible hose facilitates coupling to the helium mass spectrometer. A helium spray or a helium atmosphere under a plastic blanket will then yield a signal on the mass spectrometer for any aperture above a leak rate of 10^{-9} cc air/min.

The tape and sealing compound technique is also useful during the leak checking procedure itself. It is often easy to verify that a leak is present; pinpointing the precise location for a welding repair, however, is not always simple. By covering the leaking weld with segments of tape ribbon and sealing with compound, the search can then be quickly narrowed by spraying helium at a segment at a time while uncovering areas sequentially. It is not adviseable to apply duct sealing compound without an underlying layer of tape because the sealing compound has the potential for sealing leaks semipermanently.

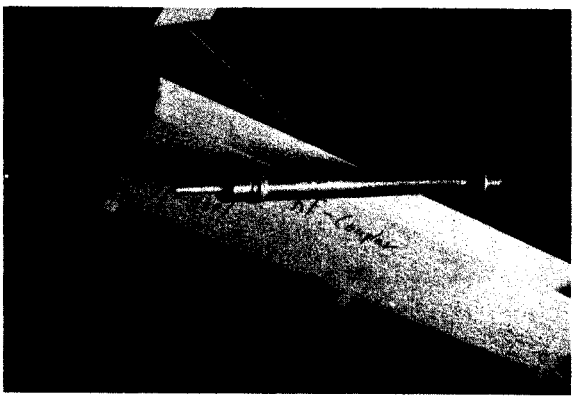

Fig. 1. The capacitive coupler between R-F transmission line and cyclotron dees is shown. Arrows mark regions where weldments are located which must be helium mass spectrometer leak tight.

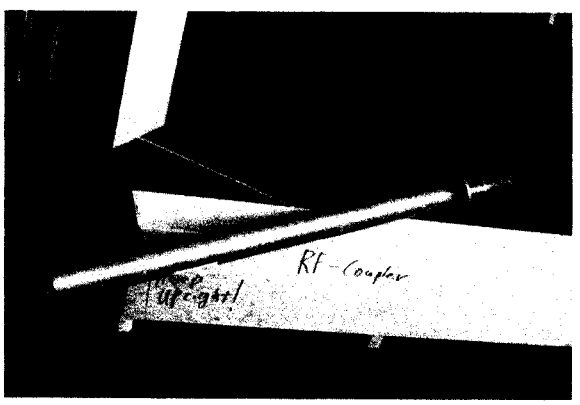

Fig. 2. A copper tube is slipped over the coupler. The right side is sealed with a rubber stopper with an adaptor for connecting to the helium mass spectrometer. The seal on the left will be completed with tape and sealing compound.

Fig. 3 illustrates the effectiveness of the technique for large scale application. To leak check the weldments of the K-800 bobbin before the superconducting wire is wound onto it, the bobbin and its outer jacket which will form the helium container for the superconducting windings, are sealed by the tape and sealing compound technique. The first step in the procedure is to lay down a supporting layer of tape which spans small apertures. A single tape layer over a 1 cm gap can easily hold one atmosphere differential pressure. The second step is the application of sealing compound over the tape so that a leak proof seal is obtained. Pumping with a 4" difussion pump, after sealing all detectable leaks, a vacuum of 5×10^{-6} torr was achieved. Since the sensitivity of the helium

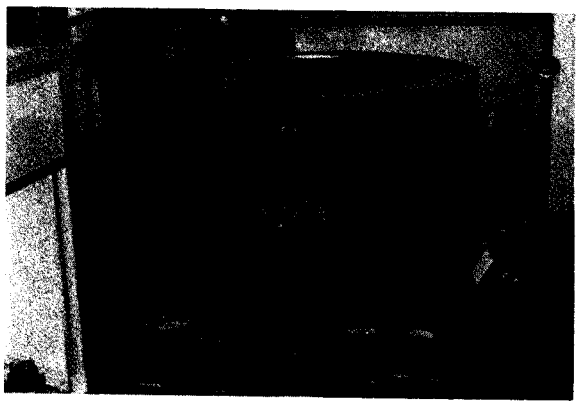

Fig. 3. The bobbin of the K-800 superconducting cyclotron is shown. The dark bands represent areas leak proofed with tape covered by sealing compound. A 4" diffusion pump achieved a vacuum of 5×10^{-6} torr. The exhaust of the diffusion pump was piped to the helium mass spectrometer for the leak checking operation.

leak detector (signal above background) is strongly dependent on the level of test chamber vacuum, this indicates that a high level of sensitivity can be achieved even when large areas are leak proofed by this technique.

---

1. Brand "NASHUA" 2" wide rolls.
2. "DUX SEAL" a product of Johns-Mansville

800 MeV Cyclotron - Main Coil Windings

D. Lawton, H. Blosser, J. Moskalik

The superconducting windings for the 800 MeV cyclotron will consist of four separate coils as shown in Figure 1. The coils will be wound in vertical layers in a spiral fashion.

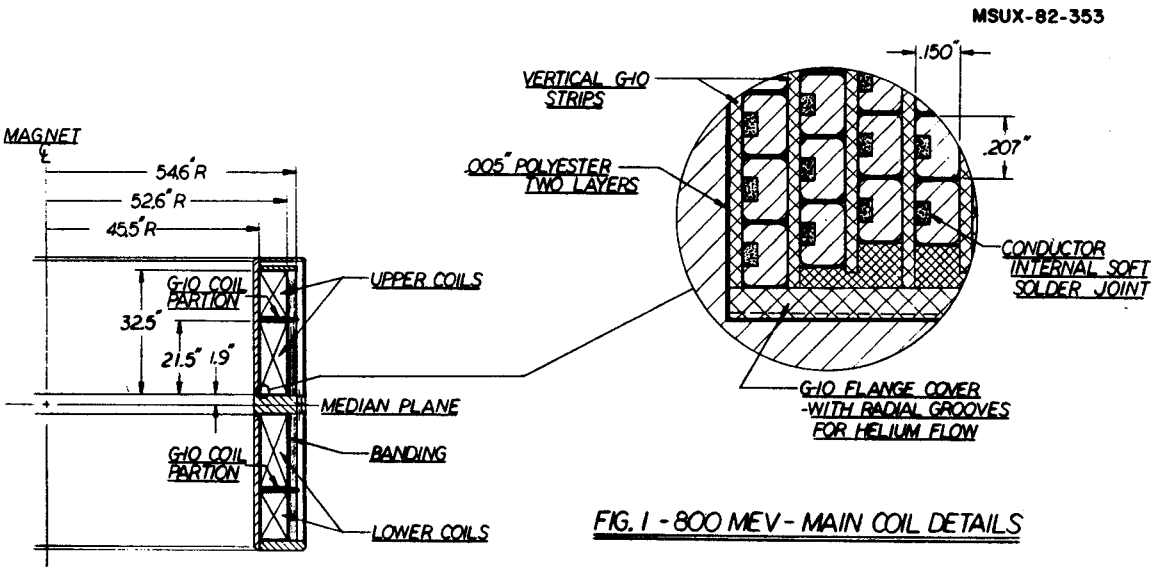

FIG. 1 - 800 MEV - MAIN COIL DETAILS

The large coils will be 32 layers with 74 turns per layer, and the small coils will be 32 layers with 49 turns per layer. The spiral shape is achieved by supporting the first turn of a layer by spacers whose heights increase gradually around the circumference to equal .215 (one wire plus insulation height) at the end of the turn. Turn to turn insulation will be provided by strips of .003 polyester film bonded with pressure sensitive adhesive onto the top and bottom surfaces of the wire. The spiral winding and the turn to turn insulation strips represent changes from the 500 MeV cyclotron main coil design. On that coil, flat turns with short climbs were used instead of the spiral, and the turn to turn insulation wrapped around the corner of the cable onto its sides. It is anticipated that these changes will simplify both the winding process and the winding aparatus. Combining this with the belief that the 800 MeV conductor is of higher quality than the 500 MeV conductor, our winding operation should be both more reliable and quicker. The coil layers will be separated radially by layers of vertical G-10 strips (dimensions -.040" x .50") positioned every 1.67^{o} around the circumference of the winding. Voids created in between the G-10 strips are flow channels for the liquid helium.

Conductor total lengths for the large and small coils will be approximately 11½ miles and 7½ miles respectively. The purchased lengths of conductor range between 2000 and 16,000 ft. Splices will be accomplished by hard soldering the copper substrate along an angled joint and then soft soldering the superconducting carrier strips back in an overlapping fashion. Tests indicate that the spliced joints have greater than 90% of the cable tensile strength.

The winding aparatus will consist of a hydraulic servo controlled tensioner to provide 3000 psi winding tension, a steam cleaning station, a submerged (water) ultrasonic transducer station to scan the cables internal soft solder joint for voids, a compressed air drying station, an insulation application station and finally a "winding arm" that serves to push on the wire both axially and radially at the point where it wraps on to the coil. All of the aparatus is mounted on a platform that is supported by the tool arm on a 10 ft. diameter table vertical boring mill. The tool arms' automatic vertical feed will allow the platform and aparatus to follow the vertical climb of the coil winding spiral. The wire winding speed will be about 20 feet per minute.

The banding for each coil will consist of 20 vertical layers of 5052-T34 aluminum wire with rectangular cross section - .215 high x .100 wide. A second tensioner will be added to the winding line to produce the required 20,000 psi tension.

At this writing, (August 1982) the superconducting cable is in house, the bobbin is in house and in its final leak checking tests, the first shipment of G-10 coil insulation parts is due in, the coil winding aparatus is being designed and fabricated in house and the banding wire is on order. The winding aparatus should be assembled and debugged in late 82' with winding proceeding in the Winter of 83'.

K800 Injection Studies

F. Marti

The original studies of the injection of the K500 beam into the K800 cyclotron were done assuming that the stripping mechanism should be placed in a hill (Ref. 1) if it were possible to do so. This limitation was imposed to avoid having the mechanism inside the dees that occupy all three valleys. To satisfy this requirement it was necessary to modify the sector geometry. It consists of a positive spiral of 1/13 inch constant up to a radius of 15 inches where it reverts to a negative spiral with the same constant. There is a 2 inch transition region between both spirals.

After examining in greater detail the possibility of designing a stripping device that would fit inside the dee, it was decided to study again the possibility of using injection in the valleys and using a sector geometry similar to the one used in the K500 cyclotron. This geometry is simpler to manufacture and does not have that transition region that somewhat reduces the vertical focusing frequency. As explained in Ref. 1, the basic requirement that the RF frequencies in both cyclotrons be the same determines the stripping radius:

$$R_s = R_{ex_1} \, h_2/h_1$$

where R_s = stripping radius, R_{ex_1} = extraction radius in first machine, $h_{1,2}$ = harmonic numbers in the K500 and K800 respectively.

HCR (h_1/h_2)	5:1	4:1	3:1	7:2	5:2
R_s (inches)	5.2	6.6	8.8	7.5	10.5

At a radius of approximately 130 inches there will be a magnet to steer the beam a few degrees toward the stripping foil. We would like to avoid having to move this magnet in azimuth to steer different ions. This requires that all beams must originate from a fixed point outside the cyclotron at that radius.

The following ions were used as test particles in our studies:

Ion #	Typical Ion	Q_2/A	E_2/A	Q_1/A	HCR
1	O^{2+}-O^{8+}	.5	200	.125	3:1
2	N^{2+}-N^{7+}	.5	200	.143	3:1
3	Ne^{3+}-Ne^{10+}	.5	200	.15	3:1
4	B^{1+}-B^{5+}	.5	200	.1	4:1
5	C^{1+}-C^{6+}	.5	200	.083	5:1
6	N^{2+}-N^{7+}	.5	140	.143	3:1
7	Ne^{3+}-Ne^{10+}	.5	140	.15	3:1
8	B^{1+}-B^{5+}	.5	140	.1	4:1
9	C^{1+}-C^{6+}	.5	140	.083	5:1
10	U^{13+}-U^{48+}	.2	47	.0546	7:2
11	U^{9+}-U^{38+}	.16	30	.0378	4:1

Where we have considered a high energy field (.5/200), a low field (.5/140) and a high field (.2/47) cases, the basic difficulty is the wide range of magnetic fields and charges of the injected ions that must be stripped in a narrow region near the center of the machine. The stripping mechanism must be kept well inside the dee, away from its edge. The stripping angles required for each of the stripping radii covered a larger region than the one provided by the present stripping mechanism. This device must be modified to safisfy the present requirements. We do not expect significant deterioration of the radial and vertical phase spaces with the new geometry.

1. Bellomo G., E. Fabrici and F. Resmini, IEEE Trans. Nucl. Sci. Ns-26 (1979) 2090.

Bobbin

H. Hilbert, R. Welton and P. Fighter

The construction of the bobbin was done through a consortium of companies which included G & L Corp. of Grand Rapids, Michigan, and Ryerson Steel and Lasker Boiler Engineering of Chicago, Ill. Lasker Boiler was mainly responsible for the work.

The bobbin itself consists of rings and flanges manufactured from special 316 stainless steel welded together using 310 stainless steel rod. Lasker Engineering rolled and welded both top and bottom cylinders, the three segments of each top and bottom flange, the top ring assembly to its ring, the bottom flange to its ring and the center flanges to their proper locations.

At this time the bobbin consisted of two separate sections with the workmanship in the range of excellent. The welding was accomplished using the highest standards of the trade with each pass being ground and dye penetrant checked. At each run out, a trough was made so that the end of the weld fell past the zone of parent material. The rollings were re-rolled and straightened after welding so that when the time for machining came, the removal of material was very uniform.

When the time came for the top and bottom sections to be welded together, Laskers' troubles became overwhelming for them. The center section has a tolerance of .040 inch and during one inspection the plates were out of position more than .500 inch.

Laskers tried the technique of using large jacks to distort the configuration so that after the parts were welded and the pressure of the jacks released the desired configuration would be assumed by the welded parts. After a few attempts using this method, Laskers gave up.

After Laskers abandoned the push and hope method, the lab and Laskers reached a financial agreement, with the lab assuming the responsibility to save the part and complete the work.

After the decision was made to remove the bobbin from Laskers, research was instigated to develop welding techniques that would enable us to salvage the bobbin. It was obvious that inducing pre-stress was not a method that ensured repeatable results. Therefore, a method of reducing the stress inherent to welding had to be developed. Initial tests showed a deflection of greater than 10% of the weld cross-section if welds were done using standard welding techniques. It was the stress induced by this welding that caused the center section plates to deflect greater than 1/2 inch from their horizontal position.

The welding method we employed was one which bridged the gap in such a way that no weld pass was larger than four inches. Using an M.I.G. welder, a three to four inch long bead was laid. Immediately afterward, the weld was peened with a blunt-nosed pneumatic hammer in order to remove the stress induced by the cooling metal. Care had to be used at this stage in order not to work harden the weld area. Tests using the above method showed distortions no greater than .005 inch from the prewelded location.

After welding was complete, the inside and horizontal surfaces were mapped and this information plotted on a polar graph. After analyzing the graph only one move was required to position the bobbin in the best location for machining.

Following the machining operation the outer covers were tac welded into place, a diffusion pump vacuum system installed and the total assembly made vacuum tight. This was accomplished by taping all the cracks with duct tape then covering these areas with duct seal.

Leaks were repaired using a T.I.G. welder and the vacuum in the high vacuum plumbing was in the low 10^{-6} torr region. With a leak tight system the next operation was to thermally shock the complete bobbin.

The bobbin was insulated and 1200 gallons of LN_2 was used to stress the welded structure. After the first shock, four leaks developed. These leaks were repaired and the thermal shock repeated. No additional leaks developed.

After some clean-up the K-800 bobbin is now ready for the next operation - winding of the superconducting coil.

K-800 Magnet Steel

Harold Hilbert

After the bids were analyzed, the job of manufacturing the K-800 magnet steel was given to Midland Ross's Bay City Foundry of Bay City, Michigan. NSCL supplied Bay City Foundry with a complete set of detail drawings (as opposed to the assembly drawings), which gave us the responsibility of design and Bay City Foundry the complete responsibility for fabrication.

Mr. Scott Holman, Manager of Bay City Foundry, split the work into two specific divisions: the casting and the machining. The casting of all detail was handled completely by Bay City Foundry personnel and the machining was sub-contracted to General Electric's Machine Repair Division of Detroit. The casting and the rough and finish machining of the top and bottom flat surfaces were accomplished in good fashion and within the time schedule. (It should be noted that although this flat machining was supervised by G.E., it was done at Bay City Foundry using their machines and personnel.)

The job of supervising and directing the work from 200 miles away complicated machining aspects of the job so much that for long periods of time the magnet details languished on the machine shops floor.

The breakdown in communications became so great that trips were scheduled and made to inspect finished work that in reality had not yet reached the final machining stage. Numerous and significant errors were made during this period with the largest being three 12 inch holes bored in the wrong locations. The correction of machining errors and correcting inperfections was accomplished at a remarkably slow pace.

Finally with the following errors and omissions the magnet arrived at the laboratory in Aug.-Sept. 1982, months late.

1. Gouges and dents caused by poor handling such as the use of chains on unprotected surfaces.
2. The omission of 48 C'bores on the outer circumference.
3. On many details, but on detail No. 3 in particular, the 7 1/2 inch C'bore was machined incorrectly.
4. Detail No. 3, 1"-8NC holes mislocated.
5. Inner surfaces on details 13, 14, 15, 16, did not meet dimensional specifications.
6. Weld repair done at sub-contractors' sites required reworking.

The repair work and the alignment of the magnet is now being accomplished.

Design Study for a 200 MHz, 50 MeV, Proton Cyclotron

Bruce Milton and Henry Blosser

At present, high power R.F. transmitters are commercially available with frequencies in the FM band (110 MHz) and at 200 MHz (for linacs). This suggests studying the feasibility of a small superconducting cyclotron for medical use, to operate at 200 MHz. Running protons in third harmonic at this frequency would require a central field of 43.413 KG. At this high field level the crucial question is whether a final energy of 50 MeV (at 8.9") can be obtained with sufficient vertical focusing.

The parameters available to adjust vertical focusing are valley depth, pole width and the spiral. It has already been shown[1] that the optimal pole width in a high field magnet is in the neighborhood of 45°. In order to allow room for the dees, which sit in the valleys, a design with poles which start with a 33° width at the center, taper to 46° at five inches, and then remain constant, was chosen. This is basically a scaled down version of the K500 pole shape. Flutter will not increase significantly by deepening the valleys once their depth is comparable to the perpendicular distance between hills. If the spiral was to be the same as that in the K500[2], then no improvement should result from making the valleys deeper than nine inches.

With these parameters set at values corresponding to maximum flutter, the spiral constant "α" (as defined by $\theta(R)=\theta_o-R/\alpha$) is the only parameter left to search in. The results of such a search are shown in Figure 1, where the maximum energy at which ν_z could be held above .1 is plotted as a function of $1/\alpha$. The conclusion drawn from this was that the spiral constant in the inner half of the machine should be greater than 1/4, and should rise to a value of 2/3 at the outer edge. In order to maintain continuous first derivatives, a function of the form $\theta(R)=\theta_o-R/\alpha-(R-R_c)^2\ \alpha'$ was chosen, where R_c is the radius at which the equation changed from $(R)=\theta_o-R/\alpha$. A value of R_c=7.25" was found appropriate for maintaining a fairly constant value of ν_z. The resulting pole design is shown in Figure 2. The predicted focusing frequencies ν_r and ν_z are shown in Figure 3. It should be noted that the only resonance would be a ν_r=1 near the center.

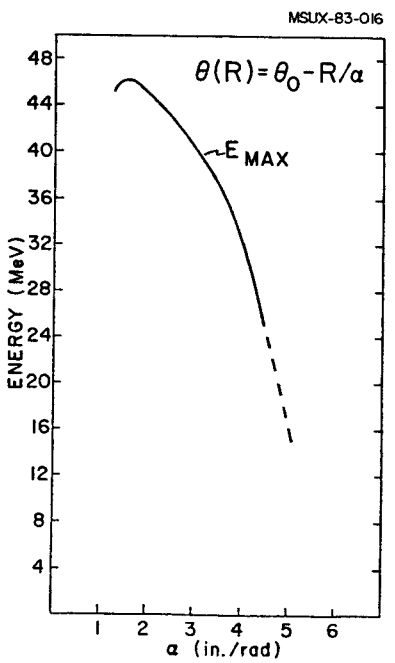

Fig. 1. Maximum focusable energy.

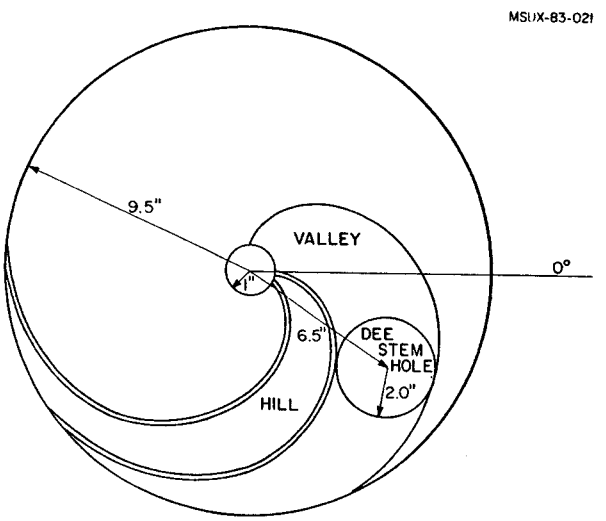

Fig. 2. Pole tip layout.

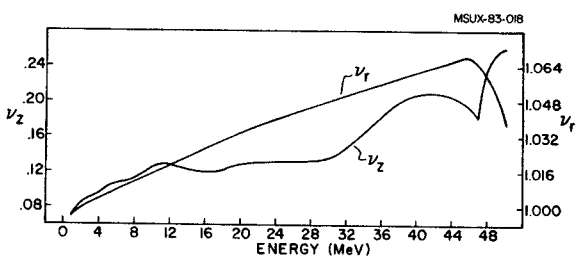

Fig. 3. Vertical (ν_z) and Radial (ν_r) Focusing.

Conclusions,

1) Little increase in the flutter can be made by further tightening the spiral, changing the hill width, or deeping the valleys.

2) The vertical focusing frequency ν_z produced by this design is most likely insufficient, since the 'hard edge' approximation used in these calculations over estimates the flutter.

3) Such a tight spiral will present problems with the dees. As can be seen in Figure 2, there is insufficient room for a two inch radius dee stem hole in the valley. Also the outer edge of the dee is approximately one quarter wavelength away from the dee stem, which would result in large voltage gradients along the dee.

4) The necessary average magnetic field, as shown in Figure 4, rises quite sharply, and most of this would have to come from the air core form factor of the coil, since most of the possible valley shimming has already been accounted for. Other similar tricks with the iron such as increasing the pole width will decrease the already low focusing.

5) Such a cyclotron, although marginally possible, would not be practical to build.

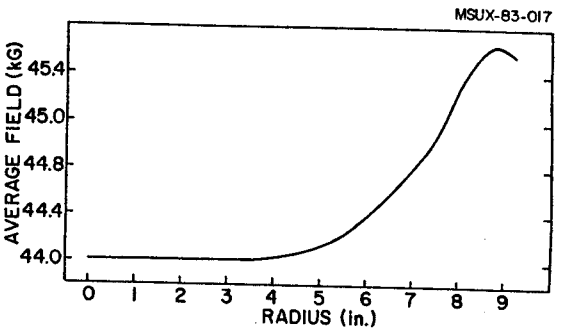

Fig. 4. Average Magnetic field from sources other than the poles.

1. H.G. Blosser, D.A. Johnson, Nuclear Instrument and Methods, 121 (1974) 301.
2. G. Bellomo, F.G. Resmini, Nuclear Instruments and Methods, 180 (1981) 305.